



The Space Telescope European Coordinating Facility Begins its Activity

P. Benvenuti, ST-ECF

As announced in the *Messenger* No. 31, on the 23rd of February 1983, the Directors General of the European Southern Observatory and of the European Space Agency signed the Agreement concerning the establishment of the Space Telescope European Coordinating Facility (ST-ECF). One year later, on the 1st of March 1984, the ST-ECF began its activity on the ESO premises in Garching.

It should be recalled that the prime purpose of the ST-ECF is to enhance the capabilities within Europe for the scientific use of the Space Telescope and of its data archive. Indeed the ST-ECF shall become the European focal point of ST related activities: it will coordinate the development of ST-related data analysis software in Europe and with the Space Telescope Science Institute in the U.S., develop original application software for the reduction and analysis of ST data, create an efficient means of archiving, cataloguing, retrieving and disseminating non-proprietary ST data, provide a convenient source of detailed knowledge in Europe of the modes of operation and performance of the Space Telescope and of its complement of scientific instruments. Depending on availability of resources, it will also provide European ST users with limited access to the ST-ECF computer time and software, in particular for those who do not have their own data reduction facilities.

In order to provide an efficient service, the ST-ECF should be able to communicate with the User Community in a timely manner. We are therefore planning to issue a quarterly ST-ECF Newsletter which will be distributed free to all the interested parties. For the time being, we asked the *ESO Messenger* to host this article as a precursor of the Newsletter.

A more direct and technical communication channel, via computer link, is under consideration with those European Centres and Networks which are more involved in the development of data analysis software.

At present, the ST-ECF staff on board is limited to the Head (the author), formerly IUE Observatory Controller at VILSPA, Madrid, the Deputy Head, Dr. Rudolf Albrecht, formerly of Space Telescope Science Institute, and the Secretary, Miss Britt Sjöberg. Dr. T. Courvoisier, now at the EXOSAT Observatory in Darmstadt, has been appointed as one of the Instrument Information Scientists and will take up duty in June. All the remaining vacant positions have been advertised and the recruiting activities are under way; we are aiming to complete the staffing of the ST-ECF by mid 1985. Our organization is shown in Fig. 1; it consists of two groups: one is responsible for monitoring the status and performance of ST and its instruments, and for designing specific algorithms and application tasks for the reduction of ST data. The second group is responsible for the coordination and development of data analysis software and for the archive system.

The prime interface for the activity of the ST-ECF is the ST Science Institute in Baltimore. First contacts have been already established and we are now aiming to set up an effective collaboration in the areas of development of application software, performance of scientific instruments and data archiving. It is expected that the ST-ECF staff will regularly spend part of their time at the ST Scl, in order to maintain an up-to-date knowledge of the ST project.

Please be informed that ESO-Chile has a new postal address:

EUROPEAN SOUTHERN OBSERVATORY (ESO)
Casilla 19001
Santiago 19
Chile

The activity of the ST-ECF has so far been devoted to the preparation of an implementation-development plan, to the recruiting of personnel and to the definition of the Host System (High Level Command Language) within which the ST application software will run. The latter point is of great importance to European users and we are therefore aiming at a thorough, albeit quick solution. The problem will be discussed with those responsible for the major European Centres and Networks in forthcoming meetings and workshops and details on the matter will be published in the first issue of the ST-ECF Newsletter.

I would like to conclude this first, short information note on the ST-ECF by saying that we will be happy to answer any questions you may have on our activity and we look forward to your suggestions and comments. Please do not hesitate to contact us: our extensions at ESO are 290/291 (P. Benvenuti) and 287 (R. Albrecht).

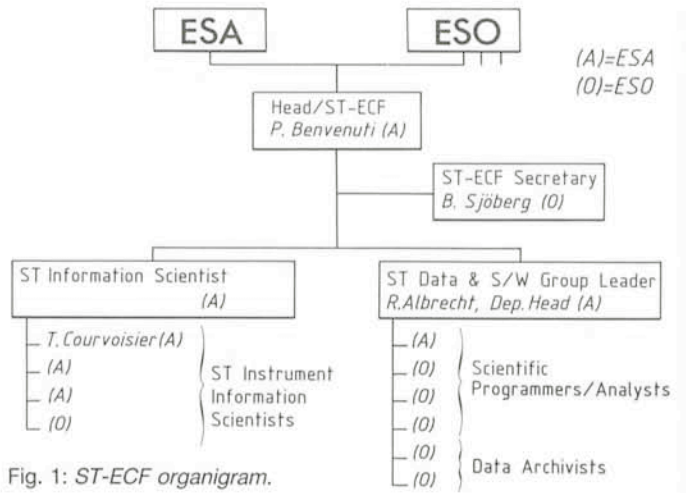


Fig. 1: ST-ECF organigram.

Progress in High Resolution Spectroscopy Using a Fibreoptic Coudé Link

G. Lund, ESO, and R. Ferlet, Institut d'Astrophysique, Paris

Experiments with a prototype 40 m optical fibre link between the 3.6 m telescope and the CES have already been described in the *Messenger* No. 31, and by Lund and Enard (1983). Further tests of this system, carried out in February 1984 using slightly different optical fibres and a highly efficient image-slicer, have confirmed the usefulness of a fibre link as an alternative to a 4-mirror coudé train. Gains in sensitivity typically of the order of 1.5 magnitudes in comparison with the classical CAT-slit-CES combination were obtained, thus permitting for the first time good spectra of 11th magnitude objects to be achieved with a resolution of 80,000.

New Fibre and Image Slicer

The new fibre link differs from the prototype tested in November 1982 only in the types of fibre and image-slicer used; two similar fibres, types QSF 133/200 AS and QSF 133/200 ASW, were tested at several wavelengths between 3900 Å and 10025 Å. These fibres were selected for their high purity silica composition, for their expected optimal transmission at respectively "red" and "blue" wavelengths, for their high degree of beam aperture conservation and for their core diameter of 133 μm which corresponds to 2.6 arcsec on the sky at the 3.6 m telescope prime focus.

When projected onto the image-slicer, the 10.5 times magnified image of the fibre output end is divided into four slices as shown in Fig. 1. The total height of the reassembled slices just matches that of the Reticon pixels. This arrangement is achieved by designing the image-slicer so as to provide a slice width of around 350 μm, corresponding to a spectroscopic resolution of 83,000 at 5000 Å. The use of a fibre larger than 133 μm would necessarily imply a loss either in resolution, or in geometrical efficiency at the detector. In preparation for the future commissioning of a new short (F/2.5) camera + CCD detector at the CES, a larger 200 μm core fibre was installed simultaneously with the other two. Although this new mode of operation will limit the spectral resolution to 35,000, the use of a larger fibre will not only enable a larger (4 arcsec) effective sky diaphragm to be employed, but will also improve the overall system transmission by around 15%.

The image-slicer tested in the recent tests is of the "Modified Bowen-Walraven" type, to which our attention was first drawn by Tom Gregory at La Silla in 1982. The slicer, as depicted in Fig. 1, consists of 3 optically polished and molecularly adhered silica elements in which the incident light is either directly transmitted, or totally internally reflected until it reaches the exit condition at the other side of the slicer. If the slicer is carefully made, transmission losses (excepting Fresnel reflections at the input and output faces) can be as low as

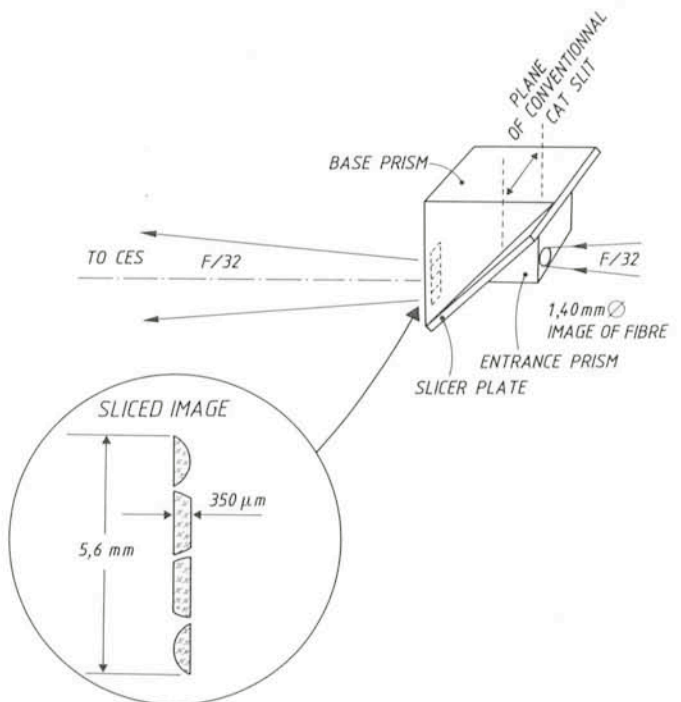


Fig. 1: Modified Bowen-Walraven Image-Slicer at the input to the ESO high resolution CES. The slicer matches the 10.5 times magnified image of the output end of an optical fibre to the rectangular configuration of the Reticon detector pixels.

4%. The slicer acts similarly to a thick parallel plate, in which the first slice of the input spot is transmitted directly and the remainder of the spot is transmitted in translated slices of which the n th undergoes $2(n-1)$ internal reflections. Experience has shown that this image-slicer is relatively easy to install, particularly since the fibre output end is immobile and can be conveniently fed with a white calibration source for daytime alignment of the slicer.

Photometric Comparison of the CAT with the 3.6 m Telescope + Fibre Link

Despite many foreseen difficulties involved in the photometric comparison of spectra obtained via the CAT with those derived by means of the fibre link, such measurements were nevertheless attempted during the first part of the recent test period. Since an effective slit width of $350 \mu\text{m}$ was imposed by the nature of the image-slicer, the CAT was used with a slit setting of the same value in order to achieve an identical resolution in both sets of observations. Spectra were thus recorded, sequentially, from the CAT and then from each of the two fibres, at ten different wavelengths using the bright stars δ^2 Vel, α Vir, and S Car. These stars were selected for their essentially smooth continuous spectrum at the chosen wavelengths and, in addition, in the case of S Car, for reasons of astronomical interest.

The read-out noise corrected, raw spectra obtained from both telescopes were reduced together in the same way; the relative gain $\gamma(\lambda)$ of the fibre link + 3,6 m over the CAT is defined as the ratio of these reduced spectra. These values are

Tentative Time-table of Council Sessions and Committee Meetings in 1984

October 8	Scientific Technical Committee, Chile
November 13-14	Finance Committee
November 27-28	Observing Programmes Committee
November 28	Committee of Council
November 29-30	Council

All meetings will take place at ESO in Garching unless stated otherwise.

plotted in Fig. 2, together with a curve (solid line) representing the theoretical gain if the fibre alone were to contribute to the system losses. The effective efficiency (righthand ordinate) corresponding to these curves is determined simply by dividing the gain (given by the lefthand ordinate) by the ratio of the collecting areas of the two telescopes (taking into account the reflection efficiencies of 0.90 and 0.98 for the two additional mirrors present in the CAT coude train, and allowing for the central obstructions of respectively 1.58 m and 0.47 m for the 3.6 m and 1.4 m (CAT) telescopes). This factor is equal to 6.82 (2.1 magnitudes).

The Influence of Seeing

Although the above figure was used to calibrate the efficiency ordinate in Fig. 2, it should be remembered that this

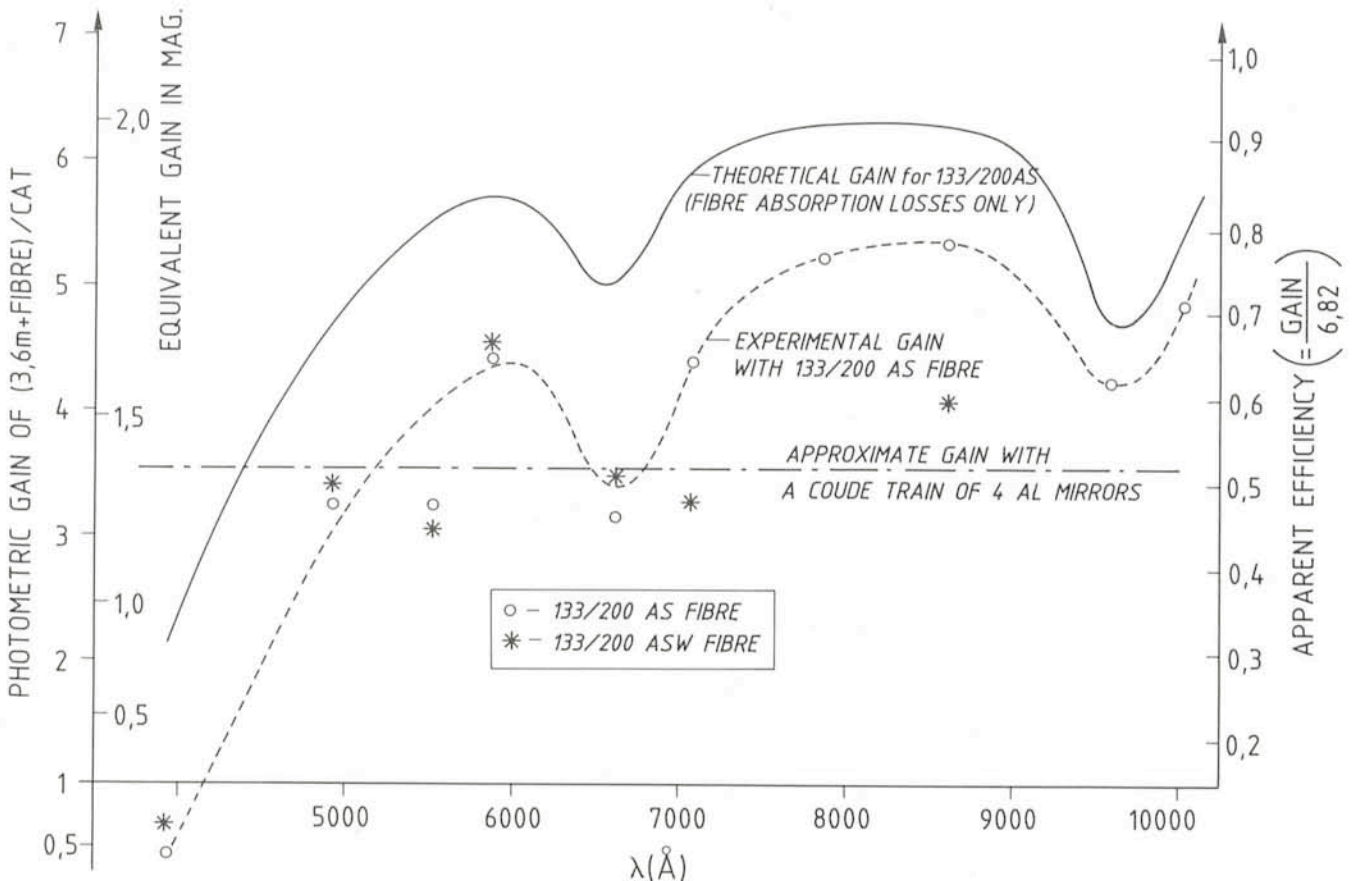


Fig. 2: Photometric gain (and equivalent efficiency) for the 3.6 m telescope + optical fibre link, when compared with the CAT. The experimental points (including a dotted-line interpolation for the AS fibre) are compared with the theoretical transmission efficiency of the AS fibre alone. The difference between the two curves is accountable mainly from the combined efficiencies of the optical beam transfer elements (Fig. 3), equal to around 71%. The gain to be expected from a conventional coude mirror train is also indicated.

calibration is somewhat arbitrary in the sense that it is seeing dependent, and assumes perfect guiding. Neither of these factors could be measured during the tests, and it is furthermore likely that the CAT seeing is better than that in the dome of the 3.6 m telescope. Both are certainly variable with time. If the assumption is made that both telescopes *do* have the same seeing, one can calculate (for an assumed Gaussian seeing profile) the relative geometrical efficiency of the 2.6 arcsec circular fibre sky diaphragm compared with that of the 1.64 arcsec (350 μ m) slit (assumed to be infinitely long) used with the CAT. This ratio is a function of seeing, but remains very close to unity for seeing conditions better than 2.3 arcsec.

For seeing worse than this value the fibre becomes comparatively less efficient than the slit, with a change equal to -15% per arcsec of seeing in excess of 2.3 arcsec. It is therefore likely for the seeing to have played a significant role in the comparative measurements if it was different at each telescope, or if it was the same at both telescopes but greater than 3 arcsec. The seeing factor, coupled with the unknown loss in photons due to guiding errors, is thought to account for the scatter in some of the data points in Fig. 2.

In Fig. 3 the coudé fibre link is schematically represented, including all of the optical elements involved in the beam transfer. Each element is associated with a figure indicating its estimated efficiency. With the exception of the absorption losses in the fibre itself, the combined losses due to Fresnel reflections and partial beam divergence beyond F/3 provide an efficiency of 71%. Although this figure should account for the disparity between the full and dashed curves in Fig. 2, which it does quite well up to 7000 \AA , the near-infrared performance of the link appears to have been better than expected. As already mentioned above, poor guiding of the CAT (which is generally less stable than the 3.6 m) could improve the apparent fibre link efficiency, whereas a strong increase in turbulence would have the opposite effect. Although these variables remain unknown, the dotted curve of Fig. 2 provides a reasonable estimate of the wavelength-dependent gain which can be expected from the 3.6 m + fibre link under *real* observing conditions.

Important Astronomical Results

For two years ESO has been operating the CES high resolution spectrograph together with the dedicated 1.4 m Coudé Auxiliary Telescope (CAT) using an echelle grating and

a cooled Reticon detector. The spectrograph is optimized for a resolving power of $R = 10^5$, corresponding to an entrance slit equivalent to nearly 1 arcsec on the sky. When the spectrograph is used under these conditions, an object cannot be observed with an adequate S/N ratio if it is fainter than about the 9th magnitude. The availability of a fibre link from the larger collecting area of the 3.6 m telescope thus opened up the possibility of observing fainter objects, up to the 11th magnitude at very high resolution. On the other hand, for the observation of much brighter objects exhibiting rapid line profile variations and requiring very high S/N ratios (~ 400), a considerable gain in time resolution can be achieved with the fibre link. This could be very useful for the study of non-radial (high order) stellar pulsations.

In Fig. 4 we present an example of very promising spectra obtained at La Silla during the recent fibre link tests. The two LMC stars R127 and R128 were observed with integration times of respectively 6,000 and 9,000 seconds, with a measured spectral resolution of 70,000. These spectra, obtained in the Na I D line region, are the best so far obtained (in terms of S/N ratio), for 10.5 magnitude stars at such high resolution.

It has been possible to distinguish a number of interesting features, which have been appropriately labelled in the figure. Among these, the following seem worthy of a brief description; – A feature corresponding to low velocity galactic gas is resolved into two components separated by 15 km sec^{-1} .

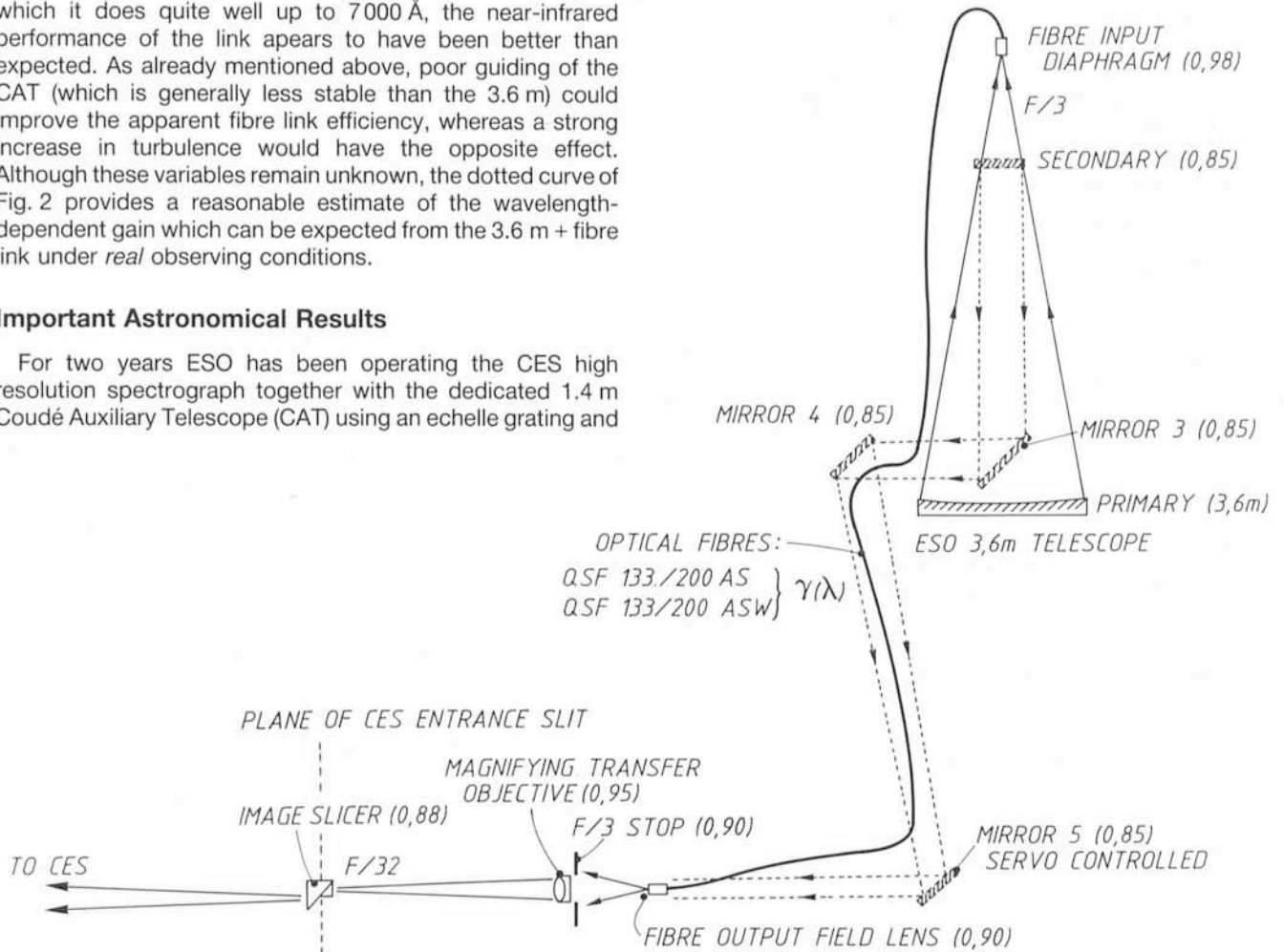


Fig. 3: Schematic representation of an optical fibre link as an alternative to a classical mirror train, for high resolution coudé spectroscopy using the ESO 3.6 m telescope. The various optical elements involved in the fibre link are associated with a figure (in brackets) giving their individual transmission efficiencies. It should be noted that the efficiency of the uncoated image-slicer can be raised to 0.95 by applying bandpass anti-reflection coatings to its input and exit faces. The alternative to the fibre (a 4-mirror train) is represented by broken lines in the figure.

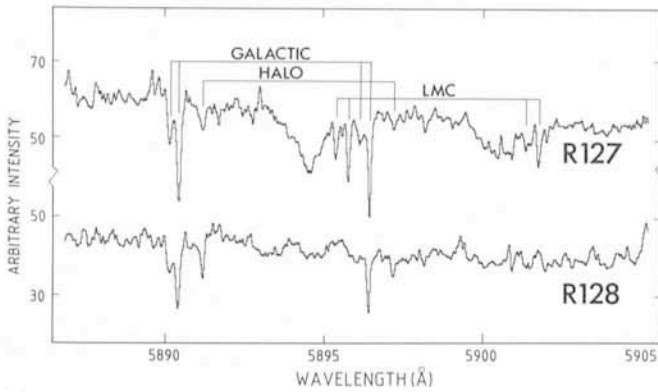


Fig. 4: Interstellar Na I D line absorption towards R 127 and R 128 in the Large Magellanic Cloud ($v = 10.5$; $R = 70,000$). Note that the ordinate is broken in order to separate the two spectra. R 127 was recently discovered to be an S Dor variable which loses enormous amounts of matter. The broad Na I D line absorption features, which are seen to be slightly blue-shifted with respect to the LMC interstellar velocities, could provide evidence of an old, cool, ejected shell. All narrow absorption features above the noise level, other than those which are labelled, are due to telluric water vapour.

– Two clearly visible Na I D components are detected in R127 at the system velocity of the LMC ($\sim +280 \text{ km sec}^{-1}$), whereas they are only marginally visible in R128. Although these stars are apparently very close in the sky, R128 may in fact be located near to the front of the Large Cloud.

– An absorption feature of intermediate velocity ($\sim +60 \text{ km sec}^{-1}$) is apparent in both stars, which could plausibly be interpreted as being due to expanding shells surrounding the LMC, formed perhaps by the tidal action of the Milky Way on the Magellanic Clouds.

These interesting results should encourage further extragalactic research using high resolution spectroscopy.

Some candidates which would now be just accessible with the 3.6 m telescope + fibre link, and which could be of significant interest if observed at very high spectroscopic resolution, are:

- galaxies, for the investigation of the morphology and physical properties of halos;
- the Magellanic Clouds, for the analysis of less evolved Magellanic material whose abundances are close to the fundamental one, or for the determination of the optical depth of the Small Magellanic Cloud;
- the brightest quasars and Seyfert galaxies, for the study of their absorption line features;
- active galactic nuclei, for the investigation of the structure in their broad line-emitting regions.

With respect to the latter, a preliminary attempt was made during the fibre tests to observe the $H\alpha$ emission line profile in the nucleus of the Seyfert 1 galaxy NGC 3783. The result of a three hour exposure is found to be most encouraging by virtue of the considerable number of emission features which are detected at various velocity displacements around the broad major $H\alpha$ feature.

Conclusions

It has been demonstrated that in spite of its considerable length, a 40 m optical fibre can provide an attractive solution for the coude spectrograph matching of a 4 m class telescope. The installation of such a system at the ESO 3.6 m telescope has enabled record sensitivities to be achieved in high resolution spectroscopy. The main additional benefits provided by the fibre link are the following:

- The onerous task of installing and aligning the alternative solution of a classical coude 3-mirror train for which (as in the case of a telescope such as the ESO 3.6 m) a servo-driven mirror may be needed, is eliminated.
- Guiding of a star onto the fibre input face is more straightforward and less prone to instabilities than with a synchronously driven coude arrangement.
- The immobility of the output end of the fibre facilitates the task of correctly aligning the beam onto the image slicer.
- The calibration lamps, which are fed through the fibre, enable all transmission anomalies of the optical system (except for that of the primary mirror), to be corrected for.
- The "image-scrambling" property of the fibre and the immobility of its output end ensure a spatially and temporally stable illumination of the spectrograph optics. This can be important for the accurate determination of radial velocities or profile equivalent widths.

The major drawback of the fibre link, as can be seen in Fig. 2, is its poor transmission at wavelengths below 4500 Å. At wavelengths above 5000 Å, however, the total link efficiency is slightly better than that of a normal coude train of perfectly aligned uncoated aluminium mirrors (this would have a combined reflectivity of 52 %). On the other hand, a coude train of interchangeable dielectrically coated mirrors could provide a highly efficient (90 %) alternative to a fibre link.

The scientific implications of the achievable improvement in limiting magnitude, when using a 4 m class telescope for high resolution spectroscopy, are discussed in the foregoing paragraph. Those areas in which important progress is likely to be made are:

- time-resolved analysis of rapidly varying features;
- the study of weak galactic and extragalactic objects (including bright quasars and Seyfert galaxies).

The potential for research in these areas should be further improved in the near future when the ESO CES is equipped with a short camera and a cooled CCD detector. Although this option will reduce the limiting resolution to around 35,000, an improvement in sensitivity in excess of two magnitudes is expected.

Future Use of the Fibre Link

Although the fibre link undoubtedly has several merits for high resolution faint object spectroscopy, its use will have to be limited to programmes of singular importance – owing to the necessary, but undesirable implication of assigning both the 3.6 m and the CAT telescopes to the observer. It is perhaps of interest to note that objects at very high declinations towards the south pole can only be observed from the 3.6 m telescope, since its dome vignettes the CAT at these declinations.

Acknowledgements

The work presented in this paper could not have been achieved without the individual contributions of many ESO staff members. In particular, we wish to thank Bernard Buzzoni and Gotthard Huster for their considerable assistance in the technical realization of this project. We extend our gratitude to Dietrich Baade, Denis Gillet and Eric Maurice for their contributions to the astronomical content of the report.

References

- Gillet, D., and Ferlet, R. 1983. *Astron. Astrophys.* **128**, 384.
Lund, G., and Enard, D. 1983. *Proc. SPIE* 445, "Instrumentation in Astronomy V", 65.

Spectroscopy of Late Type Giant Stars

A. Spaenhauer, *Astronomisches Institut Basel*, and F. Thévenin, *Observatoire de Paris*

The study of chemical abundances and their variation in the galaxy is of fundamental importance for our understanding of galactic evolution. The still unanswered questions about the dynamical and chemical evolution of the different Halo constituents (Globular Clusters, RR Lyrae stars and subdwarfs) demand for more observations of distant stars which are luminous enough to trace the halo. Considerable efforts which require extensive surveying techniques have been undertaken to accomplish this goal. As examples we mention the work of H. Bond (1980) and M. Hawkins (1984).

In this paper we describe the attempt to calibrate the broadband RGU colours of late type giant stars in terms of physical parameters. The three physical parameters describing the stellar atmosphere are the effective temperature, defined as $\Theta_{\text{eff}} = 5040^\circ/T_{\text{eff}}$, the surface gravity $\log g$ and the global abundance of metals with respect to the sun $[M/H]$. We hope that, once this calibration has been established, the wealth of the existing photographic RGU data (Basel Programme, W. Becker 1972) can be used effectively to constrain models of our galaxy and its evolution.

The programme described here is an extension of our preliminary spectroscopic observations at the Haute-Provence Observatory (Thévenin et al., 1983). We have selected 27 suspected giant stars in the three Basel fields Plaut 1 (Spaenhauer et al., 1983), Centaurus III (Spaenhauer and Fang, 1982) and a field near HD 95540 (Becker and Hassan, 1982). Fig. 1 shows the two-colour diagram of the observed

stars. The continuous line denoted with LC V represents the mean loci of disk main-sequence stars (Buser 1978). The V-shaped continuous line denoted with LC III represents the giant branch of M67 (Spaenhauer et al., 1982) which is identical with the one calculated with spectral scans (Buser, 1978).

The observations were made with the 1.52 m ESO telescope at La Silla equipped with the Echelle Spectrograph and Lallemand camera giving a resolution of $\sim 2 \text{ \AA}$. The three physical parameters Θ_{eff} , $\log g$ and $[M/H]$ have been determined with the method described by Thévenin and Foy (1983).

For the further discussion, we restrict ourselves to the colour range $1^m 50 \leq G-R \leq 2^m 15$ corresponding to the spectral type range K0 to K5, so that a total of 21 stars can be used. In order to get a photometric estimator of the metallicities of these stars, we first applied a multiple linear regression of the form $[M/H] = a \cdot (G-R) + b \cdot (U-G) + c$, which gave the formal solution $a = 3.19$, $b = -1.61$, $c = -0.58$. We therefore define $R = 3.19 (G-R) - 1.61 (U-G) - 0.58$ as the simplest (linear) photometric estimator of the metallicity. It may be useful to visualize R as defined above. When we substitute the actual colour indices $(G-R)$ and $(U-G)$ of the star in the equation above, it turns out that R is (apart from scaling) the distance of the position of the star from the M67 giant branch in the two-colour plane ($R = 3.6$ distance). The relation between $[M/H]$ and R is shown in Fig. 2. Omitting star No. 1246, which shows a large residual from the relation defined by the other stars, we arrive at the following quadratic relation: $[M/H] = -0.48 R - 0.44 R^2$ with a correlation coefficient $r^2 = 0.93$.

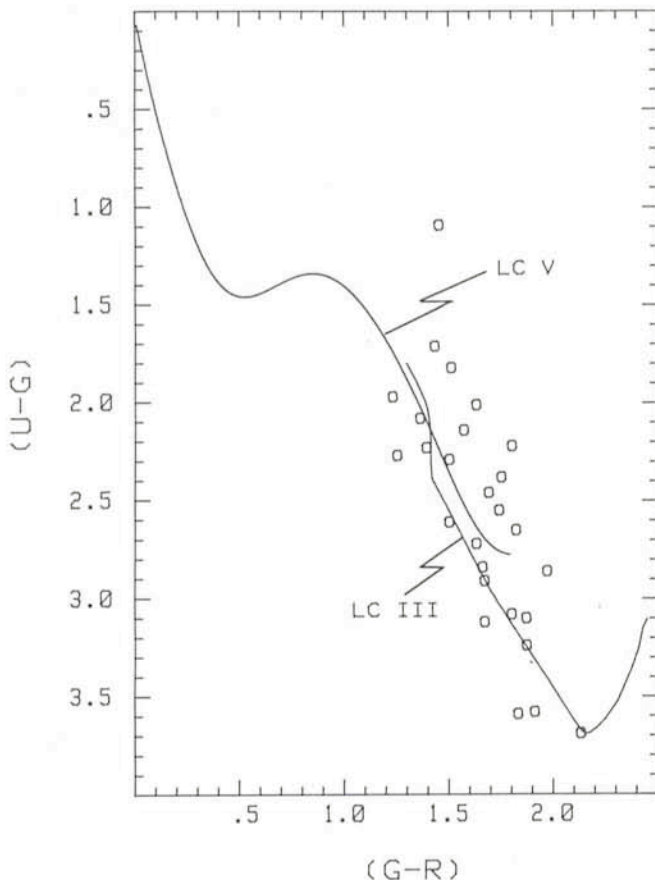


Fig. 1: RGU two-colour diagram of the programme stars. The two continuous lines represent the mean loci of disk main sequence stars (LC V) and disk giants (LC III) respectively.

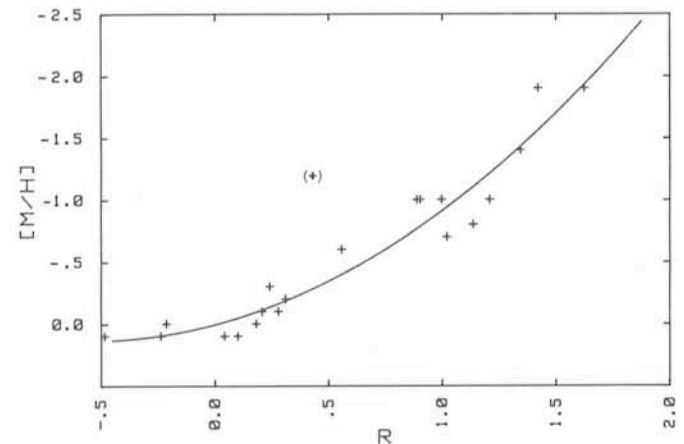


Fig. 2: $[M/H]$ versus R (broadband metallicity index, see text) diagram + programme stars. The continuous line is a quadratic polynomial regression curve omitting star (+).

Due to the increasing insensitivity of broadband colours to decreasing metallicity, this formula will no more be valid for $[M/H] \leq -2$ ($R \geq 1.5$).

It is interesting to note that there is hardly a correlation between $\log g$ and R ($r^2 = 0.01$) as well as between Θ_{eff} and R ($r^2 = 0.18$). These findings suggest that R is a metallicity indicator analogue to $\delta (U-G)$ or $\delta (U-B)$ for the subdwarfs (Wildes et al. 1962).

This report would be incomplete without mentioning the support of the technical staff and night assistants who contri-

buted essentially to the success of our observing run. Furthermore we gratefully acknowledge the financial support from the Swiss National Foundation for part of this work.

References

- Becker, W. 1972: *Quarterly Journal Roy. Astron. Soc.* **13**, 226.
Becker, W., Fang, Ch. 1973: *Astron. Astrophys.* **95**, 184.
Becker, W., Hassan, S. 1982: *Astron. Astrophys. Suppl.* **47**, 247.
Bond, H.E. 1980: *Astrophys. J. Suppl.* **44**, 517.
Buser, R. 1977: *Astron. Astrophys.* **62**, 411.

- Hawkins, M.R.S. 1984: *Monthly Notices of the Royal Astronomical Society.* **206**, 433.
Spaenhauer, A., Fenkart, R.P., Becker, W. 1982: *Mitt. Astron. Ges.* **57**, 316.
Spaenhauer, A., Fang, Ch. 1983: *Astron. Astrophys. Suppl.* **47**, 441.
Spaenhauer, A., Topaktas, L., Fenkart, R.P. 1983: *Astron. Astrophys. Suppl.* **51**, 533.
Thévenin, F., Foy, R. 1983: *Astron. Astrophys.* **122**, 261.
Thévenin, F., Spaenhauer, A., Foy, R. 1983: *Astron. Astrophys.* **124**, 331.
Willey, R.L., Burbidge, E.M., Sandage, A.R., Burbidge, G.R. 1962: *Astrophys. J.* **135**, 94.

Deep Photometry of Far Globular Clusters

S. Ortolani and R. Gratton, Asiago Astrophysical Observatory

Introduction

It is well known that our Galaxy can be represented by a flat disk and an extended approximate spherical halo.

The observed halo population consists of old, sparse stars, somewhat more than one hundred globular clusters and, in the peripheral part, some dwarf spheroidal galaxies.

While the nearest, classical globular clusters, like M 3, M 13, M 15, are the subject of extensive literature, the data concerning the outer halo clusters are sparse.

With a few exceptions these outer halo objects seem systematically different from the inner halo ones in concentration and in brightness. Their low intrinsic luminosity, combined with their large distance, explain why most of them were discovered only by the material collected during the wide field surveys with Schmidt telescopes (mainly Palomar and ESO).

While the role of the white spheroidal galaxies in the evolutionary picture of the Galaxy is not completely clear, the outer halo clusters seem the only presently observable samples of the external regions of the halo. Considering the large galactocentric distance and the low density of their environment, we may suppose that they are good "archeological relicts" of the primeval Galaxy.

About twenty star systems of this kind are known, but only four have been studied in detail. The importance of a systematic survey of them for the study of the early galactic evolution seems evident.

Observations

A general survey of distant and faint globular clusters, specifically the Palomar-Abell clusters, has been undertaken at the Asiago Observatory since 1957 under the direction of Prof. L. Rosino. However, more detailed studies require high photometric accuracy and very good sky conditions (seeing, transparency).

Thus, when Italy joined ESO in 1982, the possibility of using the ESO instrumentation at La Silla appeared very promising. The exploration of the possibilities of the new CCD detector at the Danish 1.5 m telescope seemed particularly interesting for B, V stellar photometry.

About 50 frames were obtained, under excellent sky conditions, during a four-night run in January 1983. Very good B, V pictures of the clusters Am-1, Pal 3 and GLC 0423-21 were the main results of these observations (Fig. 1-3).

The reduction was carried out at ESO's Garching computer centre using VAX/MIDAS and HP/IHAP systems. The results

show that a very good photometric accuracy was achieved at very faint magnitudes ($\Delta m = 0.1$ at $m_V = 22$).

The quality of the results is guaranteed by our tests on standard stars showing very good stability (better than 0.03 mag.). The linearity is very good, giving deviations smaller than 0.03 magnitude over a 6-magnitude interval ($17 < m_V < 23$).

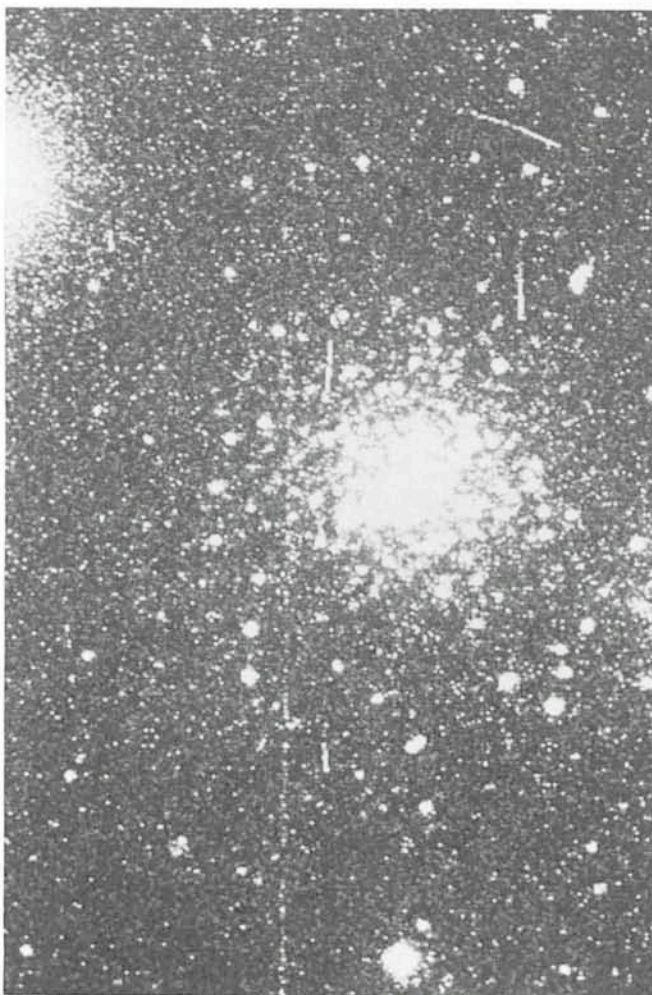


Fig. 1: B CCD image of the globular cluster AM-1. North at the top, east at right. The field is approximately $3' \times 4'$.

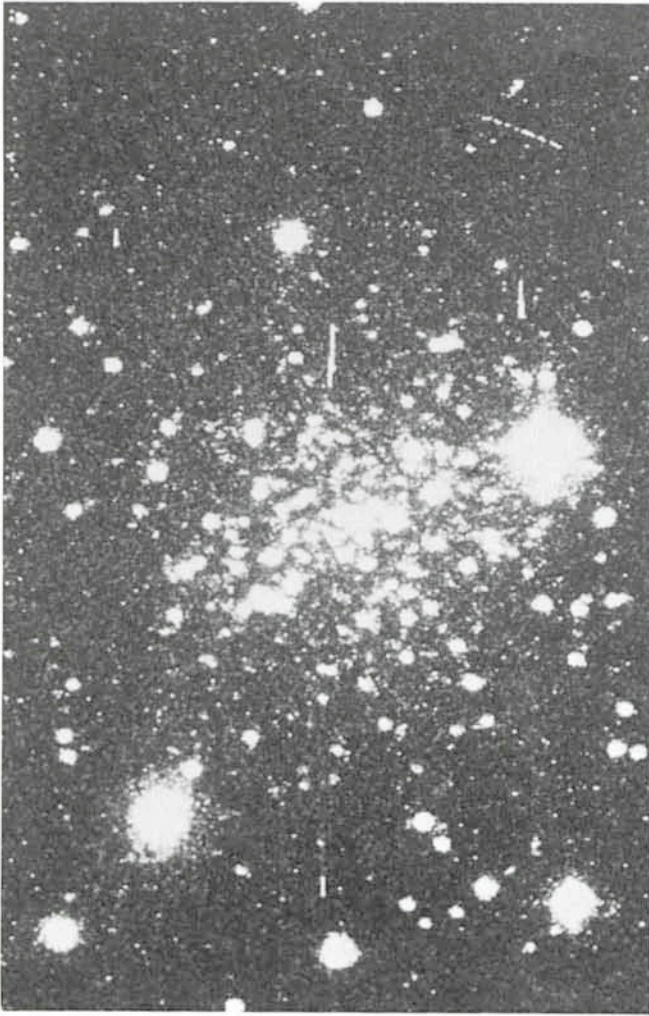


Fig. 2: V CCD image of the globular cluster Pal 3. Orientation and scale as in Fig. 1.

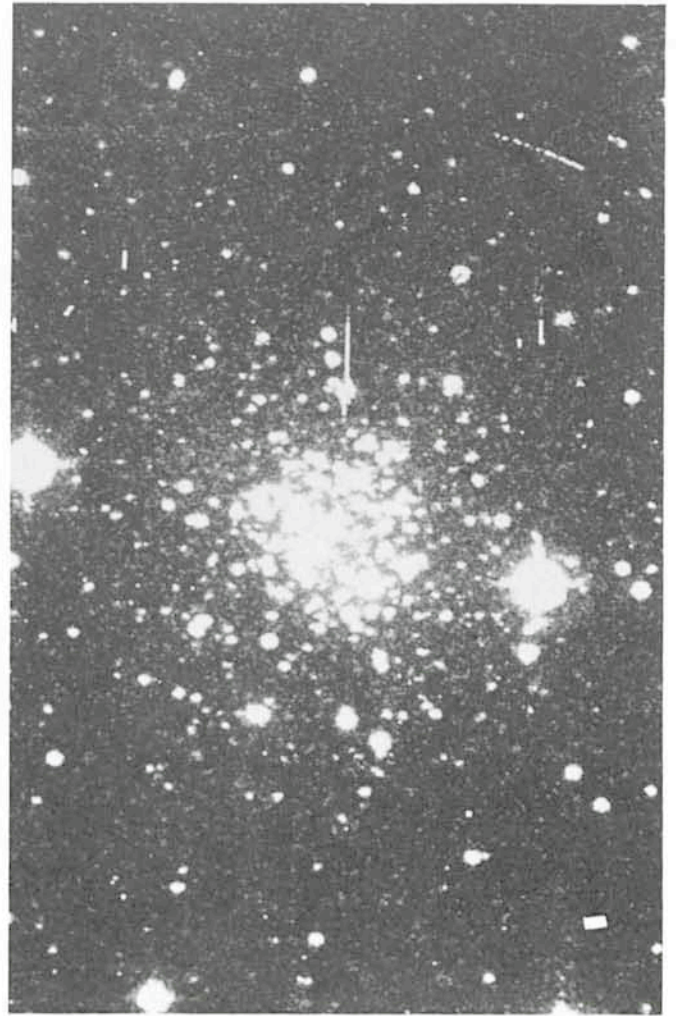


Fig. 3: The globular cluster GLC 0423-21. Orientation and scale as in Fig. 1.

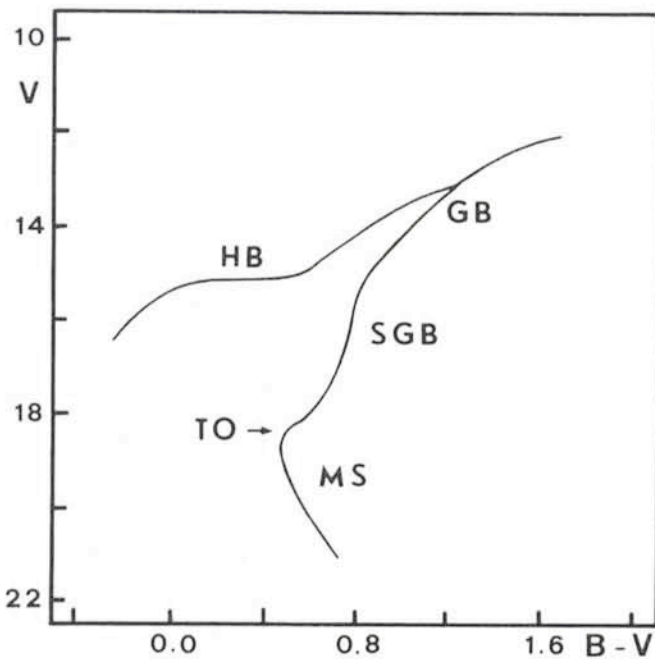


Fig. 4: Colour-magnitude diagram for a typical globular cluster. The zero point of the magnitudes is arbitrary.

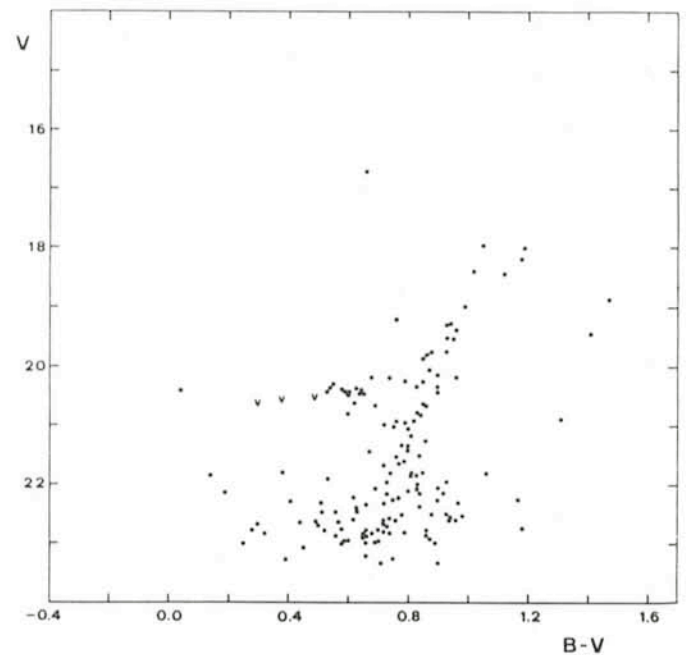


Fig. 5: Colour-magnitude diagram for the inner region of Pal 3 ($R \leq 82''$); v = suspected variables.

Results

Usually B, V photometric results on star systems are displayed through a colour-magnitude diagram (V, B-V). In a similar diagram globular clusters are characterized by the presence of a red giant branch (GB), a horizontal branch (HB) and an almost vertically descending subgiant branch to the turnoff (TO) point and main sequence (Fig. 4).

The most characteristic part of the upper region of the diagram is the HB which crosses the RR Lyrae instability strip. Its structure may strongly differ from cluster to cluster.

A change of the metal abundance was found for the inner halo clusters, in the sense that more metal poor clusters have the blue side of the HB more populated, while metal rich globular clusters have more stars in the red part.

However, a number of significant exceptions seem to indicate that factors other than the metal abundance are playing an important role (the "second parameter effect").

Fig. 5 shows the colour-magnitude diagram of Pal 3. Well defined GB, SGB and a short, predominantly red HB are present with some RR Lyrae variables, indicated by "v" symbols. Similar results have been obtained for the other two clusters. The HB structure is anomalous for intermediate metal-poor clusters like these ones. This anomalous behaviour seems to be quite frequent among outer halo clusters (Pal 14, Da Costa, Ortolani and Mould, *Astrophysical Journal*, **257**, 633, 1982; NGC 7006, Sandage and Wildey, *Ap. J.* **150**, 469, 1967) giving evidence for the importance of this mysterious "second parameter effect".

Another important result is a good distance estimate for these systems which lie at about 100 kpc from the Sun, at the frontiers of the Galaxy.

The exceedingly good quality of the data and the unexpected character of the results indicate the importance of extending our survey to other unstudied clusters at the edge of the Galaxy.

Comet P/Crommelin 1983n

A. C. Danks, ESO

Comet Crommelin has a period of approximately 27.4 years and consequently a well-studied orbit. It has an orbital eccentricity $e = 0.92$, taking Crommelin on its excursions through the solar system out to a distance of 9.09 AU and in to a perihelion distance of approximately 0.73 AU. The precise orbit details are given in IAU circular No. 3886. A comet's predicted brightness is unreliable, a function of distance from the sun, earth and albedo and naturally it is the albedo which is poorly known. But predictions for a comet with many previous passages are more reliable and the integrated visual brightness of Crommelin was predicted to be in the order of 7 to 11.

It was recognized that Crommelin would serve nicely as a test object for the International Halley Watch network (IHW), i.e. its participating observers, equipment and data compatibility. Obviously the closer the comet to the sun the brighter it becomes but of course the more it moves into day. It is usual then when the comet is brightest to catch it either in the early morning as it rises before the sun, or just above the horizon in the early evening after the sun has set.

In April and March Crommelin was well placed for observations in the southern hemisphere, reasonably bright and above the horizon in the early evening for approximately 40 to 90

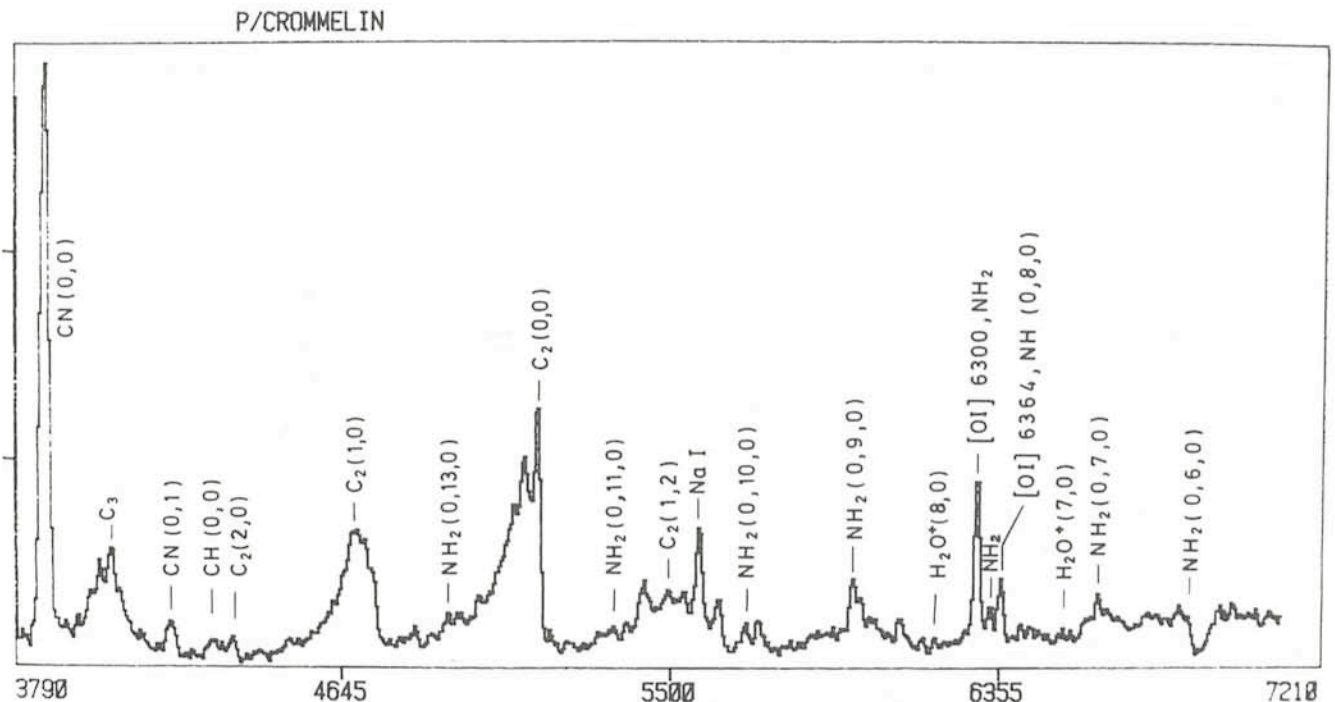


Fig. 1: A 6 minute integration on Comet P/Crommelin taken at the 3.6 m telescope on March 9, 1984 (by J. Lub and R. Grijspe), using the Boller and Chivens spectrograph and IDS detector.

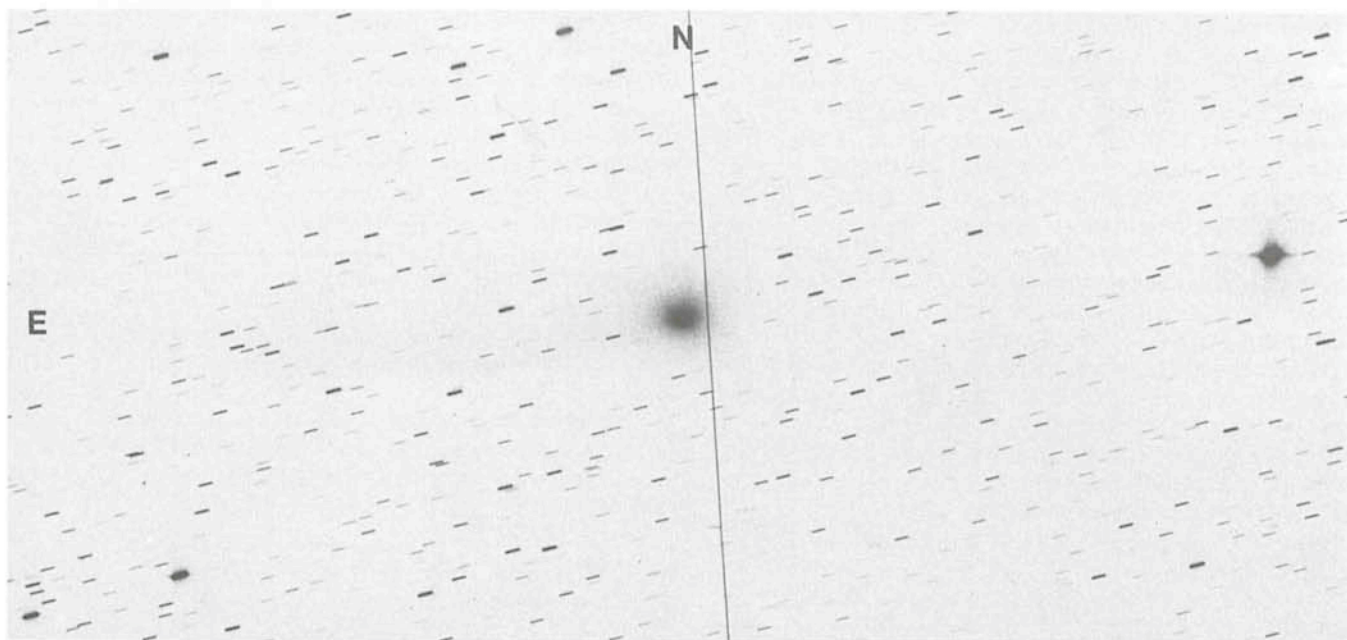


Fig. 2: Photograph of the comet with satellite trail. A 10 minute exposure taken on March 19 by H.-E. Schuster using the Schmidt telescope, 098-04 emulsion and a GG 495 filter.

minutes. Visiting astronomers at the 3.6 m, Dr. J. Lub and R. de Grijpe (Leiden) kindly agreed to include Crommelin in their observing list and made a trial integration using the IDS detector and Boller and Chivens spectrograph on March 8. The ephemeris provided by the IHW network (1984) proved very good and the comet was immediately visible in the field of the 3.6 m, moving quite quickly and with an estimated magnitude of $V = 13$ mag. A second integration 2×3 minutes was made on March 9 and is shown in Fig. 1 with the principal spectral features identified. The instrument configuration was optimized for observing emission line galaxies but was quite suitable for initial exploratory spectra of Crommelin. The two entrance apertures of the IDS subtended 4×4 arcsec on the sky and were separated by 40 arcsec. The spectrum shows the strong CN (0,0) Violet band at 3880 \AA , $C_3 \lambda 4050$ and well developed C_2 , $\Delta v = 0, +1, -1$ sequences. The other prevalent common molecule seen is NH_2 . The spectrum shown does not have the sky subtracted, however, as the second aperture was still in the comet coma but the reflected solar continuum is quite low in the blue and suggests Crommelin has a relatively low dust content. The grating used was 170 \AA/mm and gave a spectral resolution of approximately 13 \AA .

At the same time Dr. D. Cesarsky (Institut d'Astrophysique,

Paris) was observing with the recently commissioned 2.2 m telescope at La Silla, also equipped with a Boller and Chivens spectrograph but with a CCD detector. A 15 minute integration clearly showed the continuum spectrum from the comet's nucleus and emission bands from the CN (2,0) Red system.

Later, on March 19, H.E. Schuster took a fine photograph shown in Fig. 2 with the ESO Schmidt telescope. A satellite trail is seen crossing the field of view during the exposure which was made on 098-04 emulsion with a GG495 filter. The tail can be seen stretching to the east.

These are just a few of the results obtained on Crommelin at La Silla. Many visiting astronomers took spectra and carried out photometry including a group coordinated by M. Festou specifically for the HWI team. However, what is clear is that with the kind cooperation of visiting astronomers interesting and useful coverage of comets can be achieved.

I would like to thank the visiting astronomers who participated in obtaining these observations.

Reference

International Halley Watch Spectroscopy and Spectrophotometry Bulletin No. 1 (1984).

The Pickering-Racine Wedge with the Triplet Corrector at the ESO 3.6 m Telescope

G. Alcaíno and W. Liller, Instituto Isaac Newton, Santiago

Racine (1969, 1971) has revived the original idea of Pickering (1891) for extending photometric magnitude sequences on photographic plates, namely placing a slightly deviated glass wedge in the entrance beam of the telescope. This technique produces a faint secondary image next to the primary image of each bright star, and the apparent magnitude difference will be, in theory, constant over all the plate and in all colours. The

secondary images may then be compared directly with the primary images of fainter stars, thereby allowing the extension of the magnitude sequence to the plate limit.

In principle the magnitude difference Δm between the two images should depend only on the ratio of the wedge area to the rest of the beam area. However, in practice, Δm should be determined for each photographic plate since it can depend

on temporary circumstances such as the seeing, the correctness of focus, and the mirror's reflectivity directly underneath the wedge compared with the rest of the mirror. Recently Blanco (1982) and Christian and Racine (1983) have discussed the use of the wedge outlining the procedures to be followed to achieve good results.

A Pickering-Racine wedge has been available since 1979 with the Gascoigne configuration of the ESO 3.6 m telescope limited to a circular field 16 arc min in diameter, but now a wedge is available with the triplet corrector, thereby extending the field diameter to 1.0 degree. Mounted on an arm above the centerpiece of the telescope, the wedge may be moved into and out of the telescope beam by means of an on-off switch located in the control room of the dome. The wedge, manufactured by Zeiss, of Silica Herasil Top I glass, has a free aperture of 500 mm with provision for diaphragming down if required. With an apex angle of 30 arc sec, the wedge produces a separation of 14 arc sec between the primary and secondary images. The theoretically calculated magnitude difference has been given as $\Delta m = 4.0$.

On October 29, 1983, a night of high photometric quality, we tested the wedge on the telescope obtaining a set of plates of

the globular cluster 47 Tucanae and of the so-called Bok region situated in the northwestern part of the bar of the Large Magellanic Cloud. Because of the extensive range in the photometric sequences available in both fields ($8 < V < 19$), they are excellent for wedge calibration.

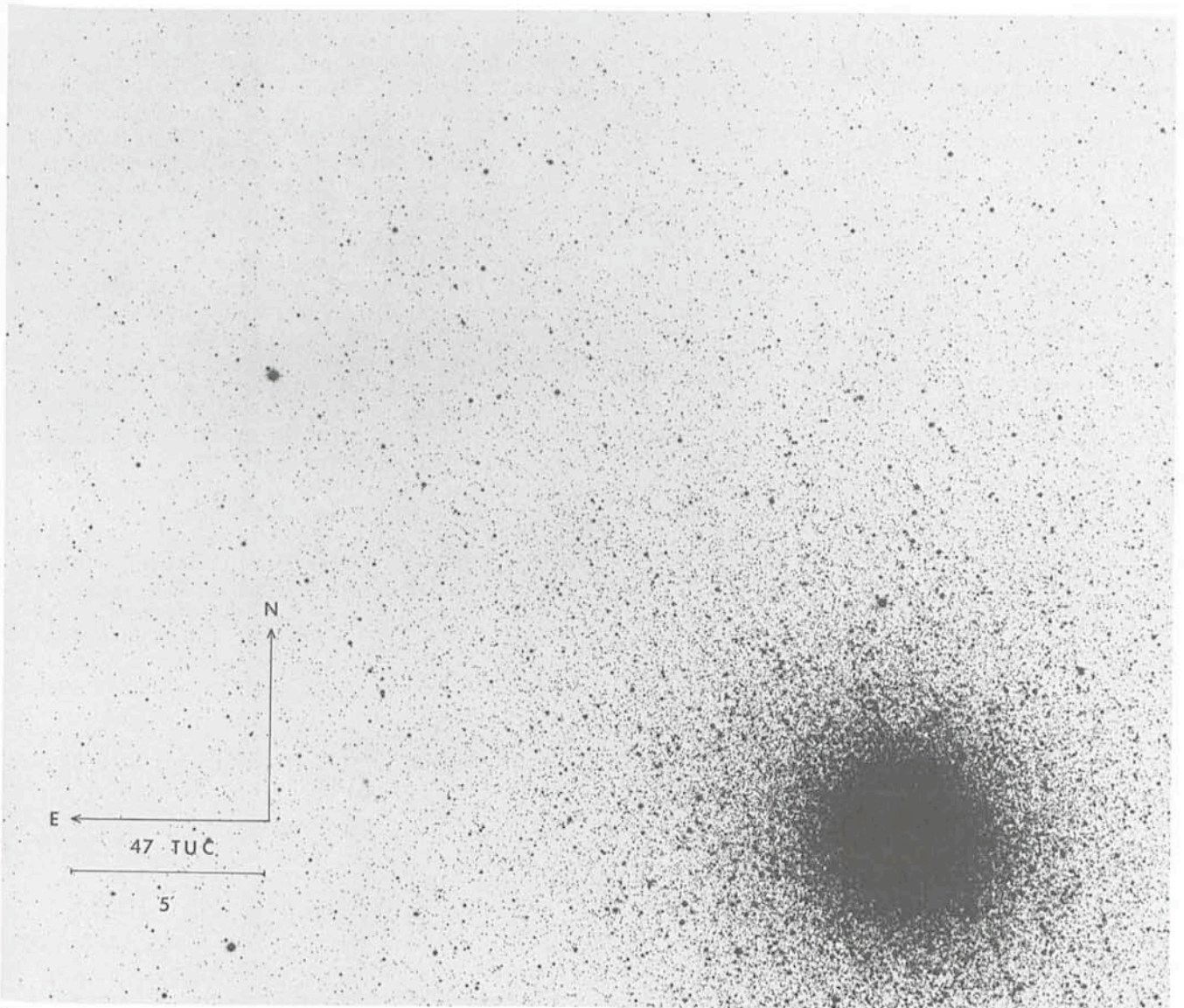
From the results from four V plates and two B plates we derive a magnitude difference $\Delta m = 4.02 \pm 0.02$. No measurable dependence of Δm on colour or magnitude or region of the plate was found.

The figure shows the northeast sector of 47 Tuc. The secondary images, displaced 14 arc sec northeast of the primary images, appear identical to the primaries in size and shape.

We are very grateful to Messrs. Ray Wilson and Francis Franza for their expert technical assistance.

References

- Blanco, V.M., 1982. *P.A.S.P.* **94**, 201.
 Christian, C.A., and Racine, R., 1983. *P.A.S.P.* **95**, 457.
 Pickering, E.C., 1891. *Ann. Astr. Obs. Harvard*, **26**, 14.
 Racine, R., 1969. *Astron. J.* **74**, 1073.
 Racine, R., 1971. *Astrophys. J.* **168**, 393.



The northeast sector of the globular cluster 47 Tucanae. The reproduction is from a 14-minute yellow plate (IIa-D + GG 495) obtained with the ESO 3.6 m telescope. Notice the secondary images produced by the new Pickering-Racine wedge, displaced 14 arc sec towards the northeast of the brighter primary images.

Finding Carbon Stars in Nearby Galaxies

M. Azzopardi, ESO, and B.E. Westerlund, Astronomical Observatory, Uppsala

Observations of remote objects in our Galaxy are severely impeded by interstellar absorption; this is particularly true in the direction of the galactic centre. Therefore, the stellar content of our Galaxy is difficult to determine except in our immediate neighbourhood; it can be estimated only by far-reaching assumptions based on local statistical studies. On the other hand, a number of external galaxies can nowadays be resolved into individual stellar members thanks to the existing large telescopes and their modern receivers. The analysis of the composition of the stellar populations of these galaxies permits conclusions regarding the correlations between their morphological structure, age, evolutionary stage and chemical composition. Studies of the distribution of various objects in the external galaxies (e.g. red and blue supergiants, Wolf-Rayet stars, red giants, planetary nebulae) provide also interesting information about changes in chemical abundance and evolutionary stage with galactocentric distance. A great advantage in this kind of studies is that, in each galaxy, we observe the various kinds of objects at the same heliocentric distance and at practically the same galactic reddening.

Survey Techniques

The first step in the study of the stellar content of an external galaxy is to discriminate its members from those of our Galaxy. The higher the galactic latitude of a galaxy is the more easily can the selection be done. Principally, three observational techniques allow the identification of members of an external galaxy: radial-velocity determinations, spectral classification, and photometric measurements. Not unfrequently all three techniques are used to prove the membership of an object. For instance, two-colour photographic photometry may be used to carry out rather deep surveys even in rather crowded regions of a galaxy. Additional photometry or spectroscopic observations may then be required to determine the exact nature of the identified objects. Frequently, objective-prism techniques (with astrographs and Schmidt telescopes) have been applied with success in areas with little crowding and on relatively bright objects; an extremely efficient extension of this kind of low-dispersion spectroscopy has been provided by the GRISM and GRENS devices on large telescopes.

In the objective-prism surveys much effort has been put into reducing the overlapping of stellar images as much as possible. For this to be achieved, unwidened spectra of lowest possible but still useful dispersion are used. A further reduc-

tion of the overlapping may result by introducing filters to diminish the spectral range observed to the minimum length which includes sufficient characteristic features for the identification of the class of objects of interest. At the same time an important reduction of the sky background is obtained, which, in turn, permits longer exposures and fainter stars to be reached. This technique has been used extensively by Azzopardi (1984, IAU Coll. No. 78, in press) to survey the Small Magellanic Cloud (SMC) for different types of luminous objects (with the ESO GPO astrograph and the CTIO Curtis Schmidt telescope). Several of the recent GRISM or GRENS surveys of external galaxies apply similar techniques.

Looking for Wolf-Rayet Stars . . .

With the purpose of extending to other nearby galaxies the surveys for Wolf-Rayet stars (WR) performed in the Magellanic Clouds with the ESO GPO astrograph (Breysacher and Azzopardi, 1979, *The Messenger* 17, 10), we have carried out observations with the ESO and CFH Corporation 3.6 m telescopes, using prime-focus triplet adaptors, GG 435 filters and a GRISM and a GRENS, respectively (see also Breysacher and Lequeux, 1983, *The Messenger* 33, 21). The GG 435 filter, in combination with the III a-J emulsion, reduces the instrumental spectral domain to the desired range, 4350–5300 Å, and at the same time appreciably diminishes the crowding. However, even with the hypersensitized plates the surveys cannot reach faint enough to reveal fully the WR population in most galaxies. So far we have discovered the only WR known in NGC 6822 (Westerlund et al., 1983, *Astron. Astrophys.* 123, 159), we have confirmed WR features in the spectra of two giant H II regions in NGC 300 and we have found numerous WR candidates in M33, whose true nature still has to be determined. We find that rather few galaxies may be explored advantageously for WR stars with the GRISM/GRENS technique. There are mainly the most conspicuous members of the Local Group, namely M 31, M 33, NGC 6822 and IC 1613 ($\langle V-M_V \rangle = 24.4$), and the major members of the Sculptor Group: NGC 55, NGC 247, NGC 253, NGC 300 and NGC 7793 ($\langle V-M_V \rangle = 27.2$). Moreover M 31, NGC 55 and NGC 253 are seen more or less edge-on and hence not ideally suited for detection of stellar members. Indeed, as the range in the luminosity of the WR stars is $-2 \leq M_V \leq -7$ (Breysacher and Azzopardi, 1981, IAU Symposium No. 99, 253) the apparent-visual magnitude ranges of these objects are $17.4 \leq V \leq 22.4$ and $20.2 \leq V \leq 25.2$ in the Local and Sculptor Group galaxies, respectively. With a limiting photographic magnitude of $V = 21$ it is clearly seen that only the most luminous WR stars may be detected, except in some of the nearest Local Group galaxies. A more efficient detector would be necessary for a complete survey of the WR stars in the Sculptor Group galaxies.

. . . and Finding Carbon Stars

During our first observing run with the ESO 3.6 m telescope we observed some fields in the Magellanic Clouds with the GRISM technique in order to obtain some standard spectra of WR stars and, at the same time, test the completeness of the previous WR surveys. We secured short and long exposures (5 and 60 min) of three fields in the Small Cloud. No more WR stars were found, but our plates contained spectra of a number of interesting objects, such as planetary nebulae, M

The Proceedings of the ESO Workshop on

SITE TESTING FOR FUTURE LARGE TELESCOPES

have now been published and may be ordered from ESO. The price for the 208-page volume is DM 25.— and has to be prepaid.

If you wish to obtain the volume, please send your cheque to: Financial Services, ESO, Karl-Schwarzschild-Str. 2, D-8046 Garching bei München, or transmit the amount of DM 25.— to the ESO bank account No. 2102002 with Commerzbank München.

giants and carbon stars. As a consequence of the low dispersion used (2200 \AA mm^{-1}) and the limited spectral range, the M giants appear as triangle-shaped continuous spectra. The carbon stars were easily recognized thanks to a marked depression caused by one of the Swan bands.

A comparison of the carbon stars identified on our plates with the aid of the C_2 band in the blue-green spectral range with those identified by Blanco et al. (1980, *Astrophys. J.* **242**, 938) and Westerlund (unpublished) in the near-infrared, also using the GRISM technique but CN bands for the identification, showed clearly that very interesting results were to be obtained from our material. We decided therefore to study the Magellanic Clouds as completely as possible and to extend our search for carbon stars to other Local Group galaxies.

What is a Carbon Star?

Carbon stars, as well as M stars, are cold and intrinsically bright objects lying on the so-called asymptotic giant branch (AGB). Carbon stars have $CO > 1$ in their envelope and atmosphere, while M stars have $C/O < 1$ and the rare S stars $C/O \approx 1$. An AGB star has a shell structure: A degenerate nucleus made of carbon and oxygen, a radiative helium layer and a convective hydrogen envelope. He burns at the base of the helium layer and H at the base of the envelope. After some time the star experiences short thermal pulses due to ignition of helium into carbon within the helium layer, and the energy liberated by this process makes this layer temporarily convective, mixing the newly formed carbon with the helium. The intensity of these pulses grows with time, and eventually the temporarily convective helium layer mixes with the convective hydrogen envelope, dredging up the carbon to the surface. If the intensity of the process is sufficient to inverse the C/O ratio from its initial value (<1) to a value (>1), the star, which was initially an M star, turns into a C star. Conventional models predict that only stars with initial masses $> 1.8 M_{\odot}$ will become carbon stars, but this limit depends on metallicity, on the extent of convective mixing and on the intensity of the helium flash (Iben and Renzini, 1983, *Ann. Rev. Astron.*

Astrophys. **21**, 271; Iben, 1983, *Astrophys. J.* **275**, L65). At least the first reason is easy to understand: The less there is of oxygen initially in the envelope, the easier it is for the star to become a carbon star, since the reversal of the C/O ratio will be easier. The two latter reasons are less obvious, although supported – at least quantitatively – by numerical evolutionary models. It appears observationally that stars with masses $> 0.9 M_{\odot}$ may become C stars in systems of sufficiently low metallicity (Bessel et al., 1983, *Monthly Notices Roy. Astron. Soc.* **202**, 59). It may be that once an AGB star has turned into a carbon star, it will not stay as such during its AGB lifetime, as evidenced by the lack of C stars amongst the brightest AGB stars: ^{12}C may turn into ^{13}C and mainly ^{14}N (with subsequent production of s-process elements like Zr) at the basis of the envelope, and the C/O ratio may turn back to values < 1 ; these objects may be the MS stars, which are M stars with ZrO bands. The evolutionary picture is complicated and still partly controversial. What is clearer is the spectroscopic discrimination between C and M stars. In M stars, all the carbon is bound in CO, and the excess oxygen forms H_2O , OH, . . . and oxides like TiO. In C stars, conversely, all the oxygen is bound in CO, and the excess carbon forms molecules like CN, C_2 , CH, . . . while oxides are absent.

Carbon Star Selection Criteria

It follows from the previous section that the bands of the cyanogen (CN) and the carbon (C_2) molecules dominate the visual spectrum of the carbon stars. They are the main characteristic features for the identification of these objects. The most prominent features are the bands of the Swan C_2 system; particularly sharply defined are the (0,0) and (0,1) bands at 5165 and 5636 \AA , respectively. Some carbon stars have also very strong bands of the CH molecule, mainly seen in the G-band. They are frequently called CH stars and form a special group.

Our selected spectral range makes the 4737 and $5165 \text{ \AA } C_2$ bands available for the identification of carbon stars. In addition, the short spectra permit an estimate or a measure-

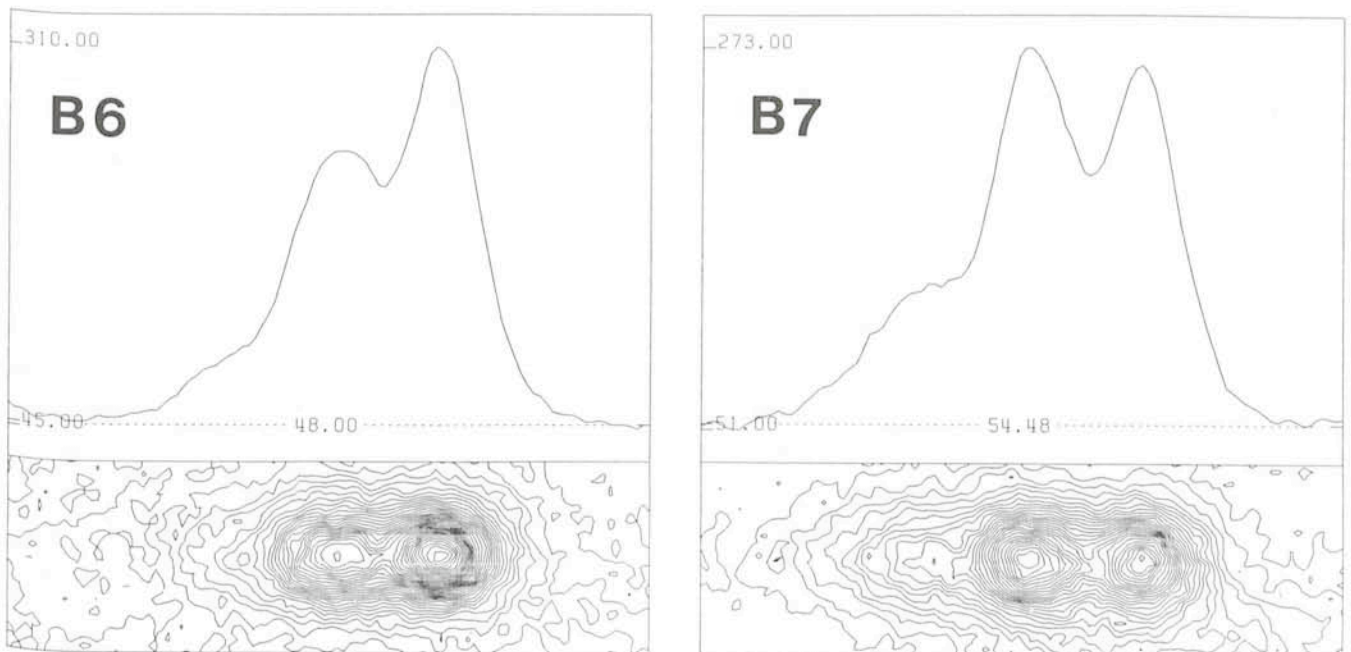


Fig. 1: Isodensity contours and intensity tracings ($4350\text{--}5300 \text{ \AA}$) of two SMC carbon stars. The pronounced central depression is the Swan C_2 band at 5165 \AA . The star B7 is clearly bluer than the more "normal" star B6. Graphs obtained from PDS scans of an ESO 3.6 m telescope GRISM plate (dispersion 2200 \AA mm^{-1}) using the Munich Image Data Analysis System (MIDAS).

The Magellanic Clouds

Blanco and McCarthy in a recent preprint have given the results of an extensive sampling of the red-star population of the Magellanic Clouds. For this, they applied the GRISM technique in the near-infrared, and used, at the prime focus of the CTIO 4 m telescope, a field of 0.12 deg^2 – except for 9 regions in the Small Cloud where a field of 0.38 deg^2 was used – to observe 37 SMC and 52 LMC regions. They covered a total of 6.8 and 6.2 deg^2 in the two Clouds, respectively, and they estimated the total number of carbon stars to be 2,900 in the SMC and 11,000 in the LMC.

Our survey, with a field of 0.78 deg^2 , will cover the main body of the SMC and give a sufficient coverage of the LMC for conclusions about the distribution over the two galaxies of the various types of carbon stars that we can distinguish from our low-dispersion GRISM spectra. Richer, Olander and Westerlund (1979, *Astrophys. J.* **230**, 724) showed that the carbon stars in the LMC could be divided into a number of natural spectroscopic groups, lying in distinct, well-defined regions of the colour-magnitude and colour-colour diagrams. The natural groups have, undoubtedly, a high correlation with the evolutionary status of the stars. Thus, we expect to be able to describe in detail the evolutionary phases of the carbon stars in the various parts of the Clouds from our material.

In order to do this, we scan the identified carbon star spectra in a PDS machine and transfer the digitized density values to intensity. We are then able to measure in our tracings: a magnitude, $m(5220)$, a colour equivalent, $m(4850) - m(5220)$, and the strength of the 5165 \AA Swan band. The latter may be expressed as an equivalent width, or a depth under the pseudo-continuum. By combining the measured quantities we can produce diagrams permitting a number of natural groups to be identified. It should also be noted that we calibrate our criteria with the aid of IDS spectra obtained with the ESO 3.6 m telescope of a number of selected stars in our fields. So far we have investigated two fields in the SMC: (A), centered at $0^{\text{h}} 48^{\text{m}}, -73^{\circ} 37'$; and (B), at $1^{\text{h}} 01^{\text{m}}, -72^{\circ} 19'$ (1950). Field A contains 306 carbon stars, field B 132. We have been able to measure 247 and 109, respectively, without disturbing overlapping. Among the group of stars that we can separate into groups are, of course, the very red and the very blue carbon stars (Fig. 1); they may then show very strong,

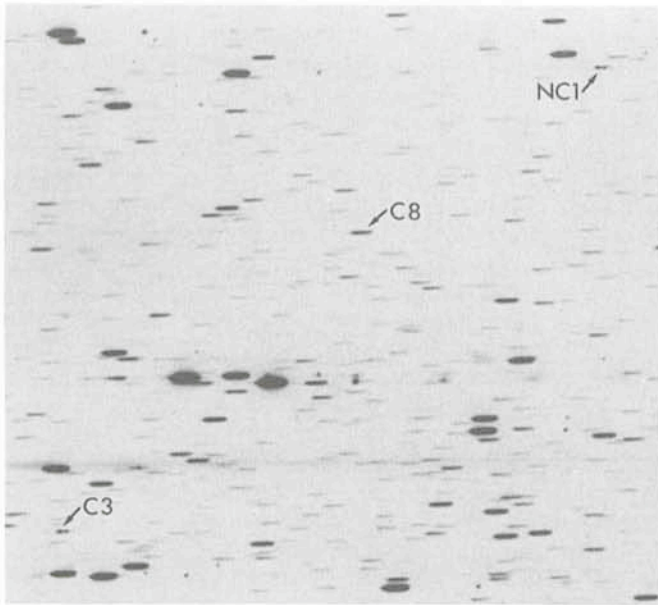


Fig. 2: The central part of the Carina dwarf spheroidal galaxy obtained, in a 2^{h} exposure, with the ESO GRISM at the prime focus of the 3.6 m telescope. The carbon stars C3 and C8 have been detected previously by Cannon and associates while NC1 is one of the newly discovered C stars (see text). The strong depression of the Swan C_2 band at 5165 \AA appears clearly in the spectra of C3 and NC1.

ment of the colours of the stars. Likewise, modern techniques permit reliable measures of the C_2 band strengths to be obtained.

In the near-infrared spectral range, which has been used extensively for surveys for red stars, the carbon stars are identified with the aid of the CN bands at 7945 , 8125 and 8320 \AA . The use of this spectral range obviously favours the reddest carbon stars, whereas surveys using the 4350 – 5300 \AA range favour the bluer ones. It is, thus, not obvious that identical samples will be found with the two methods.

Carbon Star Surveys

Near-infrared surveys have been summarized by Westerlund (1979, *The Messenger* **19**, 7). Since then, a number of near-infrared GRISM-type surveys have been carried out for carbon stars in Local Group galaxies (cf. Richer and Westerlund, 1983, *Astrophys. J.* **264**, 114, and Aaronson et al., 1983, *Astrophys. J.* **267**, 271). The C_2 bands in the blue-green region were used by Sanduleak and Philip (1977, *Publ. Warner & Swasey Obs.* **2**, 104) for the identification of carbon stars in the Large Magellanic Cloud (LMC); their observations were carried out with the CTIO Curtis Schmidt telescope equipped with a thin prism (1360 \AA mm^{-1} at $H\gamma$). More recently, Mould et al. (1982, *Astrophys. J.* **254**, 500) used the UK Schmidt telescope equipped with a low-dispersion prism (2400 \AA mm^{-1} at 4300 \AA) to search for carbon stars in the Carina dwarf galaxy.

Our GRISM/GRENS material permits us to identify carbon stars with the aid of the 5165 \AA band to rather faint magnitude limits. If we assume that the absolute visual magnitudes of most carbon stars fall in the range 0 to -4 , we are, nevertheless, limited to galaxies within about 0.2 Mpc for reasonably complete surveys, i.e. to our closest neighbours, the Magellanic Clouds and the dwarf spheroidal galaxies. The most luminous carbon stars may be seen in galaxies out to about 1 Mpc.

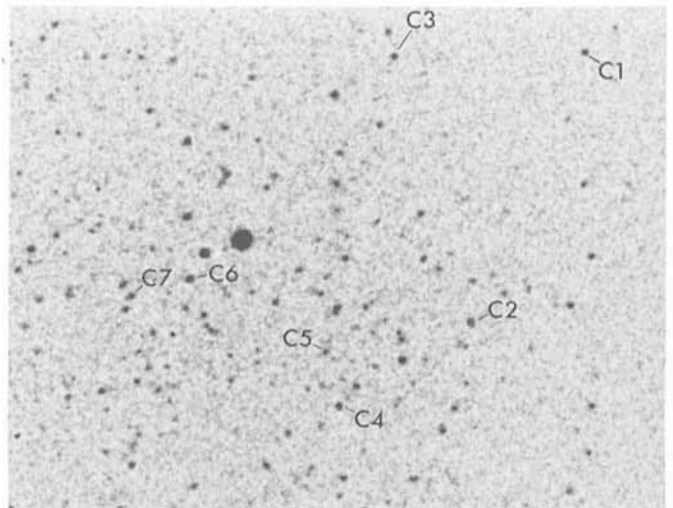


Fig. 3: Finding chart for the 7 carbon stars we detected on a CFH 3.6 m telescope GRENS plate of the Leo II dwarf spheroidal galaxy. C2 and C6 are two uncertain candidates. Copy of a part of the Palomar Sky Survey R plate No. E 1353.

"normal" or weak C₂ bands. Our IDS calibration shows also that our criteria permit the ¹³C rich J stars (Bouïgue, 1954, *Annales d'Astrophysique* **17**, 104) to be identified. We have also noted some differences between the two fields, which are in significantly different parts of the SMC. Thus, we may hope that our investigation will contribute to the understanding of the structure of the SMC, which, indeed, appears to become more and more complex (Mathewson and Ford, 1984, IAU Symp. No. 108, 125).

The Dwarf Spheroidal Galaxies

These satellites of the Galaxy appear to be old Population II systems with no evident central concentration and a noticeable lack of gas or dust. Their stars are of relatively low luminosity. Due to their rather low surface brightness their detection has been rather difficult. At present, seven dwarf spheroidal galaxies are known, namely the Sculptor, Fornax, Leo I, Leo II, Draco, Ursa Minor and Carina Systems. The last one was not found until 1977 (Cannon et al., *Monthly Notices Roy. Astron. Soc.* **180**, 81P).

The Sculptor and Fornax dwarf galaxies have been surveyed for carbon stars previously by Frogel et al. (1982, *Astrophys. J.* **252**, 133) and by Richer and Westerlund (1983, *Astrophys. J.* **264**, 114), both groups using the GRISM technique in the near-infrared. Frogel and his associates discovered two carbon stars in Sculptor and considered three more as possible carbon stars. Richer and Westerlund found the two carbon stars and added one carbon star outside the other survey. They did not confirm the three possible candidates. In our survey, which covers a larger area than the previous ones, we confirm the three known carbon stars and added three. In the Fornax galaxy, a total of 49 carbon stars were known from the previous surveys. We have now found a number of new objects so that the total number of certain carbon stars is 60 and additional 16 may be considered as possible carbon stars. The total numbers of carbon stars known in the two galaxies agree thus rather well with the estimates by Richer and Westerlund, 5 and 64, respectively.

In the Carina dwarf galaxy, Cannon et al. (1980, *Monthly Notices Roy. Astron. Soc.* **196**, 18) discovered two carbon stars which were selected as the two brightest members. Then, by carrying out a systematic survey with the UK Schmidt telescope Mould et al. (1982, *Astrophys. J.* **254**, 500) increased the number of certain carbon stars to seven; they also suggested one possible candidate. We have found the seven carbon stars and have added three certain and one possible carbon star. We were unable to confirm the character of the possible carbon star (C8), suggested by Mould and associates (see Fig. 2).

The Draco, Leo I, Leo II and Ursa Minor systems have been surveyed recently by Aaronson et al. (1982, *Astrophys. J.* **254**, 507; 1983, *Astrophys. J.* **267**, 271). They did not detect any carbon stars on their KPNO IV-N GRISM plates of the Leo dwarf galaxies. Nevertheless, they found spectroscopically, from a selection of very red stars, one and four C stars in Leo I and Leo II, respectively. On our CFHT GRENS plates we have found twelve certain carbon stars and four possible ones in Leo I, and five certain carbon stars and two possible ones in Leo II (Fig. 3). Unfortunately, since Aaronson and his associates have not provided identification charts in their paper of the carbon stars they identified, we do not know to what extent our identifications agree.

In the Draco and Ursa Minor systems, Aaronson and his associates found three and two carbon stars, respectively, on their near-infrared GRISM plates. We have not yet had the

opportunity to observe these systems, but we expect to search them for carbon stars in the near future.

In general, the new carbon stars that we have detected are either outside the fields of earlier surveys, or bluer, and possibly fainter, than those previously found. The latter may indicate that carbon stars can form lower on the asymptotic giant branch than usually assumed.

Although the absolute magnitudes, masses and luminosities of the dwarf spheroidal galaxies are rather uncertain, it is clear that there is some relation between the number of carbon stars per unit luminosity and the luminosity or the metallicity of the galaxy in the sense that as the luminosity or/and the metallicity decrease carbon stars form more easily.

Acknowledgement

We wish to thank J. Lequeux for his helpful comments and suggestions.

List of Preprints Published at ESO Scientific Group

March—May 1984

315. W. Eichendorf and J.-L. Nieto: The Central Region of NGC 1510. *Astronomy and Astrophysics*. March 1984.
316. D. Baade, Y. Bellas, W. Eichendorf and T. Tomov: Rapid Spectroscopic Variability of the Be Star HR 9070: Evidence for Double Periodicity? *Astronomy and Astrophysics*. March 1984.
317. A. Ciani, S. D'Odorico and P. Benvenuti: The Stellar Population of the Nucleus of M 33 from an Analysis of its $\lambda\lambda$ 1200–3000 Å Spectrum. *Astronomy and Astrophysics*. March 1984.
318. V. Caloi, V. Castellani, J. Danziger, R. Gilmozzi, R.D. Cannon, P.W. Hill and A. Boksenberg: Optical and UV Spectroscopy of Blue Horizontal Branch Stars in NGC 6752. *Monthly Notices of the Royal Astronomical Society*. March 1984.
319. J. Krautter, K. Beuermann, C. Leitherer, E. Oliva, A.F.M. Moorwood, E. Deul, W. Wargau, G. Klare, L. Kohoutek, J. van Paradijs and B. Wolf: Observations of Nova Muscae 1983 from 1200 Å–10 μm during its Early Decline Stage. *Astronomy and Astrophysics*. March 1984.
320. E. Maurice, M. Mayor, J. Andersen, A. Ardeberg, W. Benz, H. Lindgren, M. Imbert, N. Martin, B. Nordström and L. Prévot: Radial Velocities of Southern Stars Obtained with the Photoelectric Scanner CORAVEL. II. Faint Southern Potential Radial-Velocity Standards. *Astronomy and Astrophysics, Supplement Series*. March 1984.
321. G. Vettolani, R.E. de Souza, B. Marano and G. Chincarini: Clustering and Voids. Read by G. Chincarini at the Beltrami Foundation Meeting, Padua. April 1984.
322. R.E. Williams and W.A. Christiansen: Blast Wave Formation of the Extended Stellar Shells Surrounding Elliptical Galaxies. *Astrophysical Journal*. April 1984.
323. P. Bouchet: The Photometric Behaviour of the Young Disk Carbon Star TW Horologii. Determination of its Physical Characteristics. *Astronomy and Astrophysics*. April 1984.
324. A. Lauberts: UBVRI Photoelectric Photometry of 191 Southern Galaxies. *Astronomy and Astrophysics, Supplement Series*. April 1984.
325. R. Bandiera, F. Pacini and M. Salvati: The Evolution of Non-Thermal Supernova Remnants. II: Can Radio Supernovae Become Plerions? *Astrophysical Journal*. April 1984.
326. R. Bandiera: Convective Supernovae. *Astronomy and Astrophysics*. April 1984.

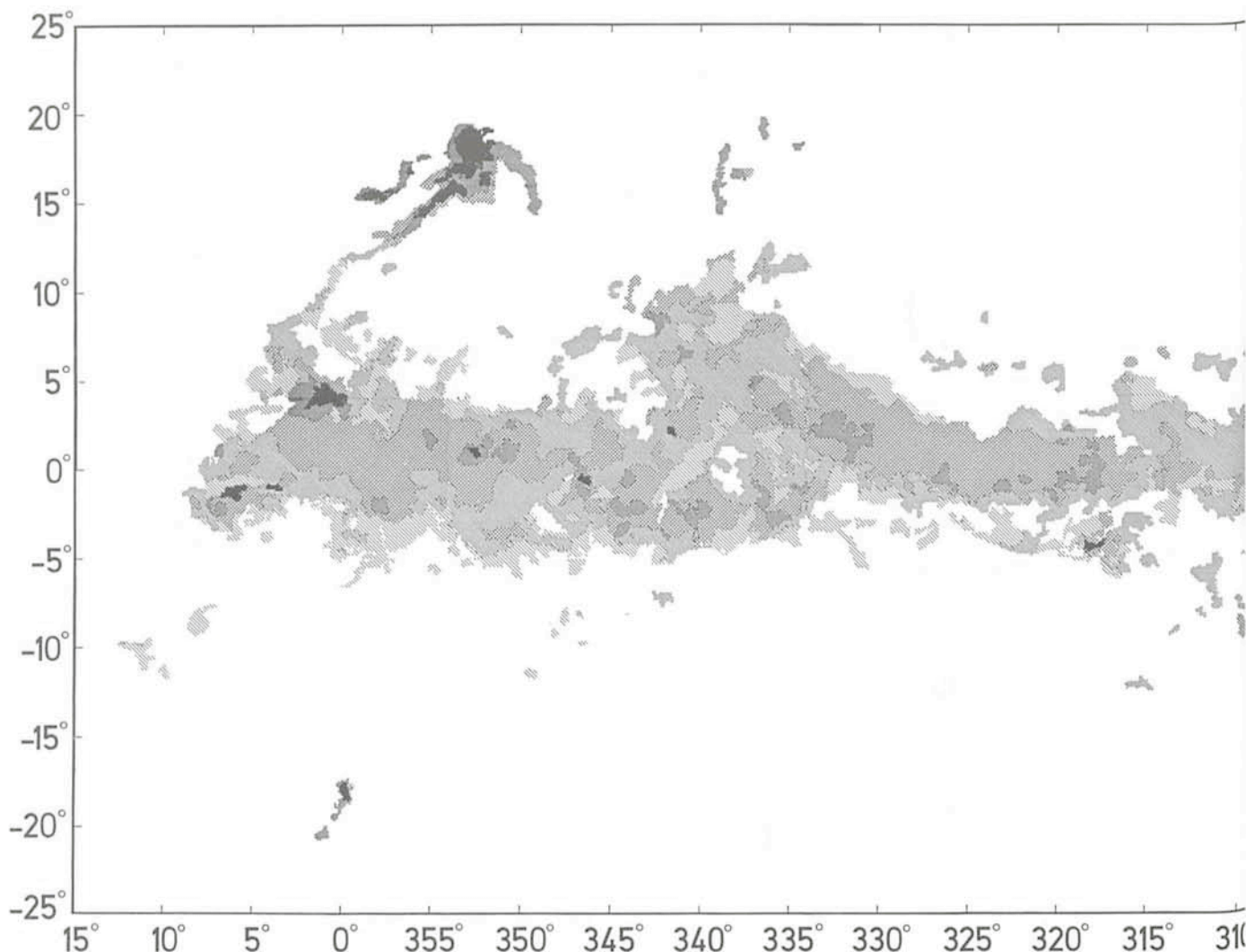


Fig. 1: The distribution of dark clouds ($> 0.01 \text{ deg}^2$) in galactic coordinates. This map exists in a machine readable, digitized form as a $500 \times 1,400 \text{ pix}$

A Catalogue of Dark Nebulae for the Southern Hemisphere

J.V. Feitzinger, J.A. Stüwe, Astronomisches Institut, Ruhr-Universität, Bochum

A catalogue of dark nebulae and globules has been compiled from a study of the ESO (B) and SRC J Sky Atlas for galactic longitudes $240^\circ < l < 360^\circ$. This catalogue closes the great southern gap open since the work of Lynds (1962) for the northern hemisphere. To secure utmost consistency and comparability between both surveys we followed as closely as possible Lynd's method in searching, determining and describing the dark nebulae.

The 606 fields of the southern atlas were examined for the presence of dark clouds; for $|b| > 30^\circ$ no dark clouds are found, although our search extended up to $|b| = 90^\circ$. The catalogue (with cross references) contains positions, sizes, opacities and the van den Bergh (1972) classification on the filamentary morphology of 489 dark clouds and 331 globules.

The overlapping regions between the POSS-Lynds survey and our work were used to calibrate our opacity classes. This linkage secures the equality of the opacity classes in both surveys, in spite of the different limiting magnitudes of the photographic material. Lynds used the red and blue POSS prints and recorded only clouds visible on both the red and blue photographs. She suspected that, by doing this, the more

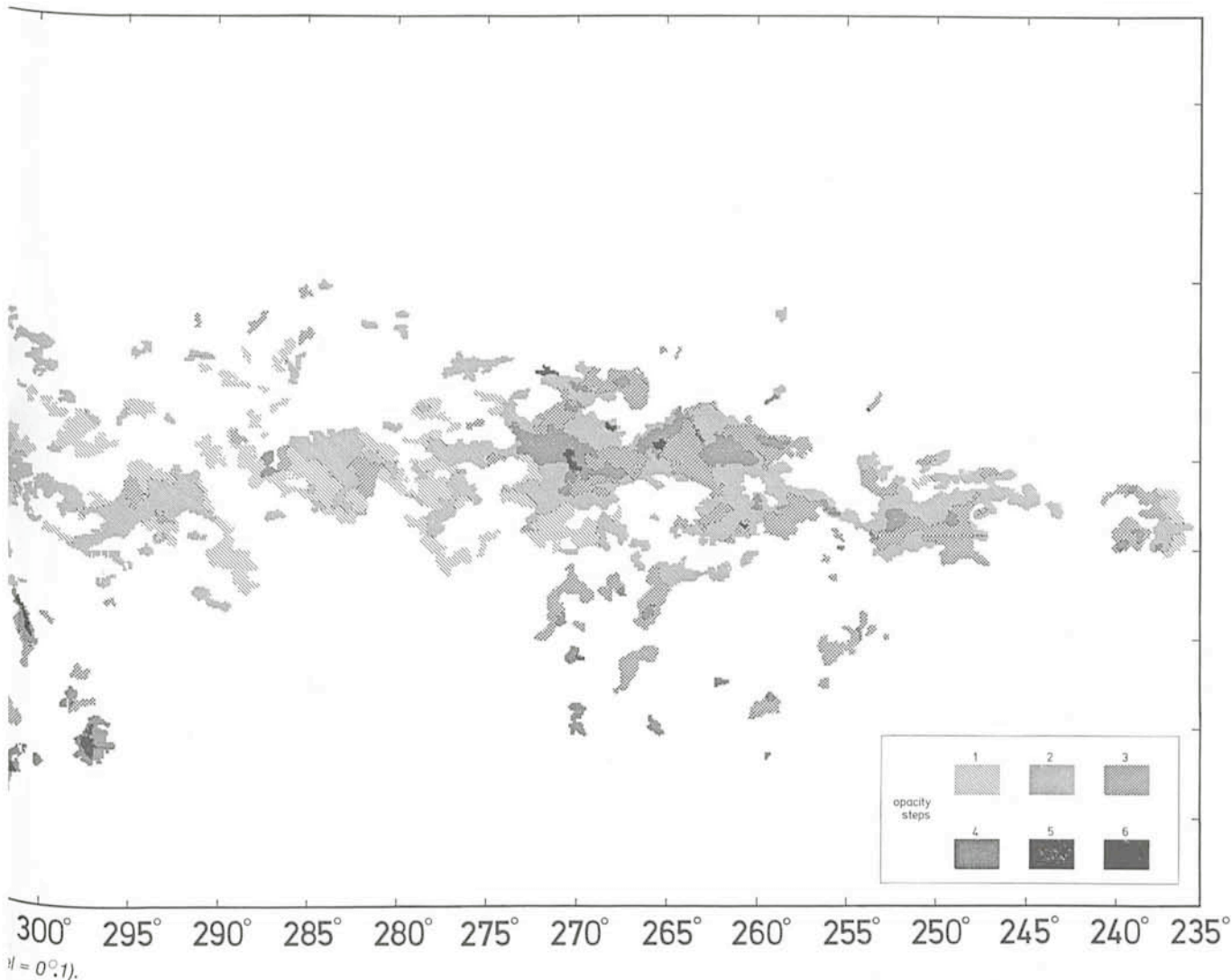
tenuous clouds, which may be transparent in the red, are not included. We have used the blue plates to obtain a greater completeness level. By comparing the clouds of the overlapping regions of the two surveys, we find that the cloud number per field is not influenced.

The percentage of the sky obscured by dark clouds is 4.98 % for the northern ($0^\circ < l < 240^\circ$) and 1.92 % for the southern part ($240^\circ < l < 360^\circ$), so the northern sky shows 2.5 times the obscuration of the southern hemisphere. The absolute numbers are (area $> 0.01 \text{ deg}^2$):

north: $N = 1273$ clouds, area = 1396 deg^2
 south: $N = 437$ clouds, area = 264 deg^2 .

This reflects the well-known fact that the visible Milky Way band changes its morphological appearance from north to south.

The southern part appears more homogeneous as a consequence of the absence of the Great Northern Rift in the Milky Way. This results in fewer clouds of high opacity, which are responsible for the ruggedness. Furthermore the southern part is much brighter, also a reason for greater homogeneity.



Besides their different opacities interstellar clouds show a bewildering variety of shapes and sizes. To take this fact into account, we supplemented the catalogue by descriptive categories: tail of a cometary globule, worm track, dark filament, etc., and the classification scheme of van Bergh (1972). The four categories: amorphous cloud (α) . . . sharp-edged absorption (δ) may be understood in terms of a simple physical picture of the evolution of interstellar clouds. These

classifications should reflect the evolutionary history of the dynamical or thermal processes that once provoked the formation of the dark clouds and globules.

References

- B.T. Lynds, 1962, *Ap. J. Suppl.* 7, 1.
S. van den Bergh, 1972, *Vistas* 13, 265.

The Chemical Enrichment of Galaxies

F. Matteucci, ESO

Galaxies are thought to have formed out of a primordial gas consisting of ~77% Hydrogen, ~23% Helium and traces of Deuterium and Lithium without heavier elements. At the present time the chemical composition of the interstellar medium (ISM) in the solar neighbourhood shows a composition of ~70% Hydrogen, ~28% Helium and ~2% heavier elements. This progressive enhancement of Helium and heavier elements at the expense of Hydrogen in the interstellar gas is referred to as galactic chemical evolution.

The chemical evolution of galaxies is governed by many factors such as the rate at which stars form, their mass spectrum, their evolution through successive thermonuclear cycles and the dynamics of the gas-star system. Each generation of stars contributes to the chemical enrichment of a galaxy by processing new material in the stellar interiors and restoring to the interstellar medium (ISM) a fraction of its total mass in the form of both processed and unprocessed matter, during various mass loss events (stellar winds, planetary nebula

ejection and supernova explosion). The next stellar generation then forms out of this enriched gas and evolves, giving rise to an ongoing process which terminates when all the available gas has been consumed.

In order to describe in detail this process of enrichment, it is necessary to know how much gas is turned into stars per unit time, the initial mass function (IMF), and how much and when nuclearily processed material is restored to the ISM by each star (stellar yields).

Since in recent years the chemical evolution of galaxies has been the subject of a great deal of theoretical work, I will not describe here the many details and intricacies of this topic, but I will present only some results:

(i) the determination of the yields per stellar generation of several chemical elements (He^4 , C^{12} , C^{13} , O^{16} , N^{14} and Fe^{56}) as a function of two important stellar evolution parameters,

(ii) the effect of the iron production from intermediate mass stars on the chemical evolution of the solar neighbourhood.

(i) The Determination of Yields per Stellar Generation

The importance of determining the yields of the chemical elements per stellar generation is that, from them, many important conclusions regarding the chemical evolution of galaxies can be drawn without considering detailed evolutionary models. In fact, under simple assumptions, the ratio between the yields of two elements gives direct predictions concerning the ratio of the corresponding abundances.

The net yield per stellar generation of a given element (He and heavier) is defined as the fraction of matter restored to the ISM by a generation of evolving stars in the form of newly created element i , divided by the total fraction of matter locked up in low mass stars and remnants.

In order to compute the yields per stellar generation we need to specify only the stellar yields and the initial mass function. The initial mass function, defined as the mass of stars contained in the mass interval $m, m+dm$, is generally expressed as a power law ($\psi(m) \propto m^{-x}$) and, for the sake of simplicity, is assumed to be constant in time.

The most important factor governing the nucleosynthesis production is the stellar mass, even if the chemical composition can be very important in affecting the yields as I will show in the following.

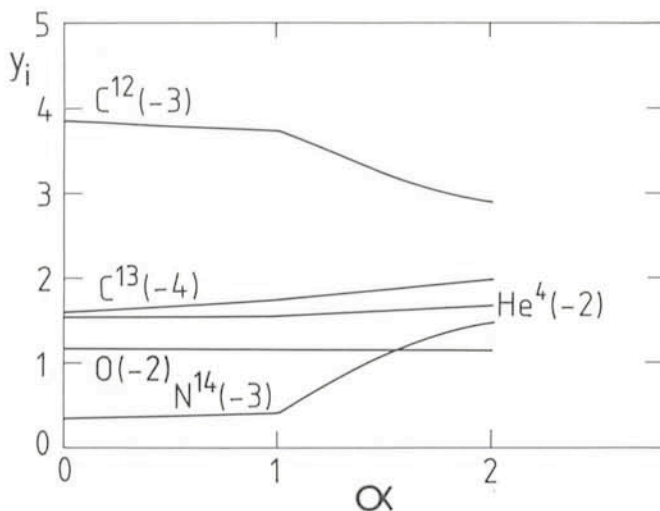


Fig. 1: Yields per stellar generation of He^4 , C^{12} , C^{13} , N^{14} and O^{16} as a function of the mixing-length to pressure scale height ratio α . The value of the mass loss efficiency parameter η is fixed and equal to 0.33.

Star masses contributing to the galactic chemical enrichment can be divided into three main categories:

(a) low mass stars ($0.8 \leq m/m_{\odot} \leq 2.3$) which develop an electron degenerate core after the Main Sequence phase,

(b) intermediate mass stars ($2.3 \leq m/m_{\odot} \leq 9$) which ignite He non-degenerately but develop an electron degenerate Carbon-Oxygen core after the exhaustion of the Helium at the centre,

(c) massive stars ($10-15 \leq m/m_{\odot} \leq 100-120$) which are able to synthesize, during the course of their evolution, all the elements from Carbon to Iron.

Low mass stars evolve through a core H-burning, a shell H-burning, a core He-burning and a double shell phase (Asymptotic Giant Branch). They essentially contribute to the enrichment of He^3 , He^4 , C^{13} , N^{14} and s-process (slow neutron capture) elements through stellar winds and planetary nebula ejection, ending their lives as white dwarfs.

Intermediate mass stars evolve through the same phases as low mass stars but can also ignite Carbon in their cores. However, if the mass loss process reduces the mass of the star below $1.4 M_{\odot}$ (Chandrasekhar mass), Carbon will never be ignited and the star will eventually become a white dwarf. On the other hand, if Carbon is ignited in an electron degenerate C-O core (which is the case for intermediate mass stars), hydrodynamical and nucleosynthesis computations suggest that a thermal runaway (Carbon-deflagration) should occur, resulting in the complete destruction of the star. During the C-deflagration some nucleosynthesis would occur and at least one half of the core mass of $1.4 M_{\odot}$ would be transformed into iron peak elements, with the composition of the remaining mass showing the presence of all the elements between Carbon and Iron (Nomoto, 1983). As a consequence, inter-

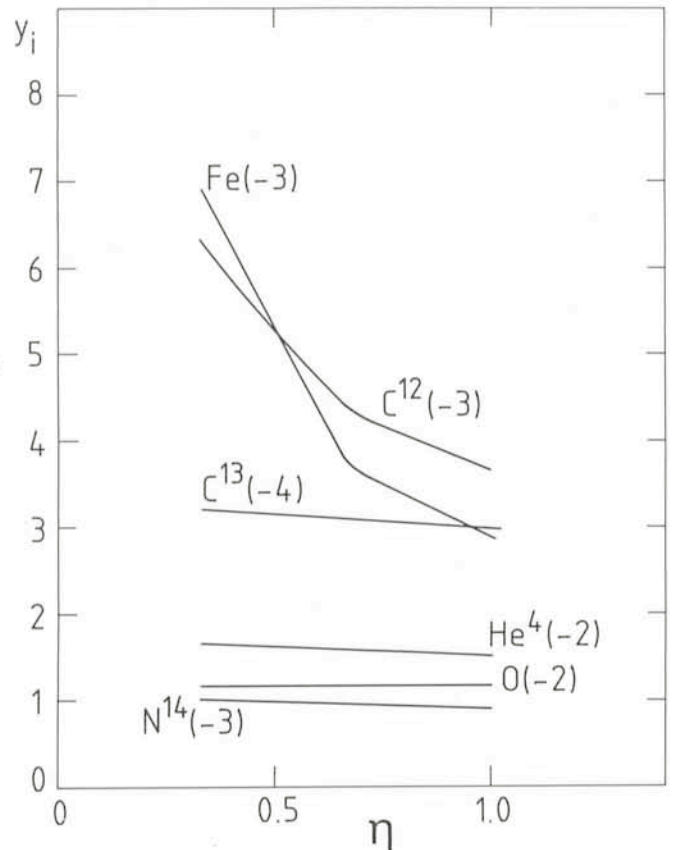


Fig. 2: Yields per stellar generation of He^4 , C^{12} , C^{13} , N^{14} , O^{16} and Fe^{56} as a function of the parameter η and for $\alpha = 1.5$.

mediate mass stars could be responsible for the production of a substantial amount of heavy elements in addition to the same elements produced by low mass stars. Unfortunately, the maximum limiting mass for which the final product is a C-O white dwarf is very uncertain, since it is a strong function of the mass loss efficiency, a quantity which is, in turn, very poorly known.

Massive stars are generally believed to be the major contributors to the heavy element production. In fact they can develop all the nuclear burnings up to the formation of a central Nickel-Iron core, followed by successive shells containing products of O- C- He- and H-burning. Massive stars contribute to the galactic enrichment through stellar winds and supernova explosions. The mass loss during the H- and He-burning phases essentially affects the Helium production; the contribution of the stellar wind to the yields of heavy elements can become important only after a certain mass limit i.e. $40-50 M_{\odot}$ (Maeder, 1981, 1983).

Fig. 1 und 2 show the yields per stellar generation of several elements (He^4 , C^{12} , C^{13} , O^{16} , N^{14} and Fe^{56}), which I computed for a given IMF ($x = 1.35$, Salpeter, 1955) and different choices of two important parameters influencing the evolution and nucleosynthesis of low and intermediate mass stars: the mixing length to pressure scale height ratio α , and the Reimers (1975) mass loss parameter η (the nucleosynthesis results concerning low and intermediate mass stars are taken from Renzini and Voli, 1981). The data concerning the chemical enrichment by massive stars are a miscellany of Arnett (1978), Woosley and Weaver (1983) and Maeder (1981), with the exception of the Iron production which I assumed to be one half of the quantity computed by Arnett (1978) as Silicon + Iron. With increasing α , the total yield of C^{12} decreases in favour of those of He^4 , C^{13} and N^{14} as a consequence of the intermediate mass stars which convert the primary C^{12} (primary elements are those synthesized directly from H and He^4), dredged-up after each He-shell flash, into primary N^{14} and C^{13} . In fact, the parameter α affects the efficiency of the burning at the base of the convective envelope (hot-bottom burning), where the fresh Carbon is converted into N^{14} and C^{13} via CNO-cycle. By varying the parameter η from 0.33 to 1 the maximum limiting mass of a star becoming a white dwarf ranges from 4.7 to $6.8 M_{\odot}$, owing to the functional relationship between this limiting mass and the parameter η (Iben and Renzini 1983, case b = 1). I have assumed that each SN produces $0.7 M_{\odot}$ of Iron, $0.35 M_{\odot}$ of Carbon and $0.35 M_{\odot}$ of Oxygen after the destruction of its core of $1.4 M_{\odot}$. With increasing η the number of intermediate mass stars suffering degenerate core carbon ignition decreases, affecting the yields of Fe and C^{12} . On the other hand, the yield of Oxygen is not very sensitive to the efficiency of mass loss from intermediate mass stars, because the bulk of this element is produced by massive stars. The yields of the other elements produced before the SN explosion (SNe) (He^4 , C^{13} , N^{14}), are not substantially affected by mass loss by stellar winds.

I want to stress the point that chemical yields are very useful for testing the stellar evolution theory: in fact, we can select among the various yields, computed under different assumptions about the stellar evolution parameters, the ones which better reproduce the observed chemical abundance ratios, as I will show in the next section.

(ii) The Iron Production in the Solar Neighbourhood

More recent results (Tornambé 1984) suggest that the rate of SNe by Carbon-deflagration can be a function of the initial stellar metal content. It has been found, in fact, that stars in the mass range $5-10 M_{\odot}$ can suffer degenerate core carbon ignition when their metal content Z ranges from 0 to 10^{-5} (first

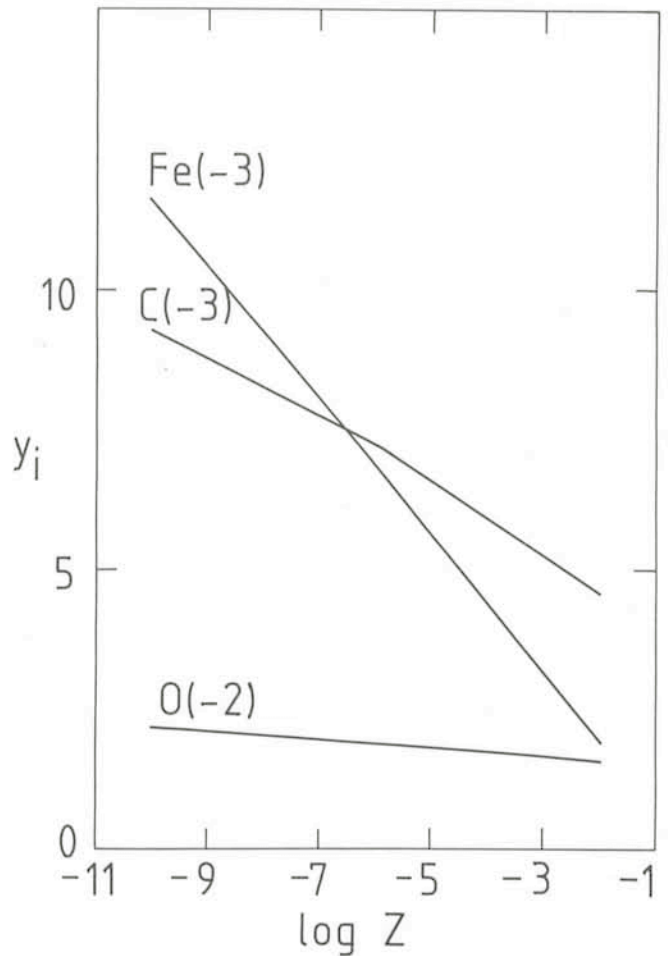


Fig. 3: Yields per stellar generation of C^{12} , O^{16} and Fe^{56} , computed following Tornambé's (1984) results, as a function of the logarithm of the metal content Z , for $\alpha = 1.5$ and $\eta = 1$.

stellar generations), whereas for larger metallicities the mass range shrinks and at the present time (solar chemical composition) only stars between 8 and $9 M_{\odot}$ are candidates to explode. This is due to the efficiency of mass loss which has been considered a function of the stellar metal content, increasing with increasing metallicity, as suggested by many observational and theoretical studies. Fig. 3 shows the yields per stellar generation of C^{12} , O^{16} and Fe which I have computed as a function of the metal content Z by taking into account the Tornambé (1984) results. The nucleosynthesis prescriptions are the same as described before with $\alpha = 1.5$ and $\eta = 1$, which I found to be the better choice for these parameters in order to reproduce the presently observed abundance ratios.

The predicted yields are decreasing with the increasing metal content, indicating that the first stellar generations produced more than the later ones. This result is due only to the influence of the stellar chemical composition on the yields, and can be very important in the study of galactic chemical evolution. For this reason I have computed the temporal variation of the Iron abundance in the solar neighbourhood. The chemical evolution model which I have used follows the evolution of the fractionary mass of a given element due to stellar nucleosynthesis, stellar mass ejection and infall of gas of primordial chemical composition; it also takes into account the temporal delay in the chemical enrichment due to stellar lifetimes, which is essential to account correctly for the contribution of long living stars. The predicted iron abundance

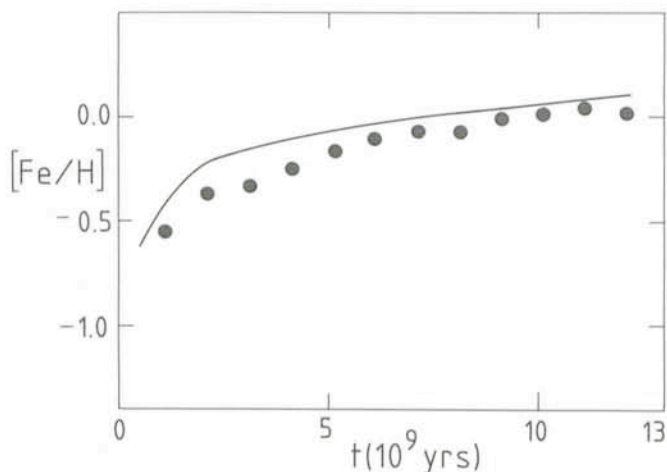


Fig. 4: The theoretical age-metallicity ($[Fe/H]$ is a logarithmic measure of the Iron abundance relative to the sun) relationship compared with the observational data of Twarog (1980) for solar neighbourhood stars (full dots). The time is in units of 10^9 years. The mean metallicity in the solar vicinity increased by about a factor of 5 between 12 and 5 billion years ago, and has increased only slightly since then.

as a function of time is found to be in good agreement with the age-metallicity relationship for solar neighbourhood stars (Twarog 1980), as shown in Fig. 4. This indicates that the Iron produced by intermediate mass stars, in addition to the massive ones, does not lead to an overproduction of this element when the corresponding yield is a decreasing function of time.

Finally, I want to mention that, from an observational point of view, the possibility that low and intermediate mass stars can produce Iron peak and other heavy nuclei is suggested by the spectra of type I SNe (Branch, 1980), which are believed to originate from this stellar mass range. However, the progenitors of these SNe are still uncertain and two classes of them can be envisaged: single intermediate mass stars and white dwarfs in binary systems (Iben and Tutukov, 1983). In both cases the nucleosynthesis products would be the same because they come from the destruction of a C-O core of $1.4 M_{\odot}$ exploding by carbon deflagration.

References

- Arnett, D.W., 1978, *Ap. J.* **219**, 1008.
 Branch, D., 1980, in *Type I Supernovae*, Ed. J.C. Wheeler, Austin.
 Iben, I. jr., Renzini, A., 1983, *Ann. Rev. Astron. Astrophys.* **21**, 271.
 Iben, I., Tutukov, A., 1983, in *Stellar Nucleosynthesis*, Erice workshop, Ed. C. Chiosi, A. Renzini, Reidel Publ. Comp., in press.
 Maeder, A., 1981, *Astron. Astrophys.* **101**, 385.
 Maeder, A., 1983, in *Primordial Helium*, ESO workshop, Ed. S. D'Odorico, D. Baade, K. Kjær, p. 89.
 Nomoto, K., 1983, in *Stellar Nucleosynthesis*, Erice workshop, Ed. C. Chiosi, A. Renzini, Reidel Publ. Comp. in press.
 Reimers, D., 1975, *Mem. Soc. Roy. Sci. Liège*, 6 Ser. **8**, 369.
 Renzini, A., Voli, M., 1981, *Astron. Astrophys.* **97**, 175.
 Salpeter, E.E., 1955, *Ap. J.* **121**, 161.
 Tornambé, A., 1984, in *Population Synthesis*, Frascati workshop, Ed. V. Caloi, V. Castellani, *Mem. Soc. Astron. It.*, in press.
 Twarog, B.A., 1980, *Ap. J.* **242**, 242.
 Woosley, S.E., Weaver, T.A., 1983, in *Supernovae: A Survey of Current Research*, Ed. M.J. Rees, R.J. Stonehan, Reidel Publ. Comp., p. 79.

Stellar Seismology: Five-Minute P Modes Detected on Alpha Centauri

E. Fossat, Observatoire de Nice

G. Grec, B. Gelly and Y. Decanini, Département d'Astrophysique de l'Université de Nice

A short note in a recent issue of the *Messenger* (Fossat et al., 1983) described the first test of a new spectrophotometer specially designed for extending to a few bright stars the results already obtained in solar seismology. Since the late seventies, we know that the sun is pulsating within a certain range of eigenmodes, the most famous having periods around five minutes. The most striking results in this field have been obtained by the observation of integrated sunlight. Indeed in this case, the angular filtering is so severe that only radial and weakly non radial (degree $l \leq 3$) eigenmodes can be observed. Their number is limited enough to make the identification possible despite the absence of any angular resolution in the observation. More than 80 of such eigenmodes, attributed to the pressure acting as a restoring force, have been thus identified in the five-minute range in the case of the sun (Grec et al., 1983). Once identified in angular degree, radial order and temporal frequency, these eigenmodes make possible a real seismological investigation of the internal solar structure (Gough, 1984).

Because important results have been obtained in integrated sunlight, observing the sun "as a star", it was tempting to try to

achieve similar results on other stars. Evidently, the 10^{11} flux reduction factor for the brightest stars makes the task highly difficult, because the oscillation amplitudes to be detected are below 1 ms^{-1} in Doppler shift measurements. It is for this special goal that we have designed a special spectrophotometer, using again the principle of optical resonance spectroscopy. The conclusion of the first test of this new instrument was that if the observation can be photon noise limited (i.e. in total absence of any instrumental source of noise), the five-minute solar oscillation could still be detected by removing the sun far enough for its magnitude to reach about zero.

Such a situation is very closely represented by the observation of Alpha Centauri A, because it is a G2 V star, very similar to the sun, with a mass of $1.1 M_{\odot}$. Six nights were granted to this programme on the ESO 3.6 m telescope, 22–28 May 1983. Two and a half nights provided over 20 hours of data of photometric quality good enough for analysis. In fact these data consist of two signals:

- The monochromatic intensity (about 0.08 \AA bandwidth) in the red wings of the Na D1 and D2 lines.

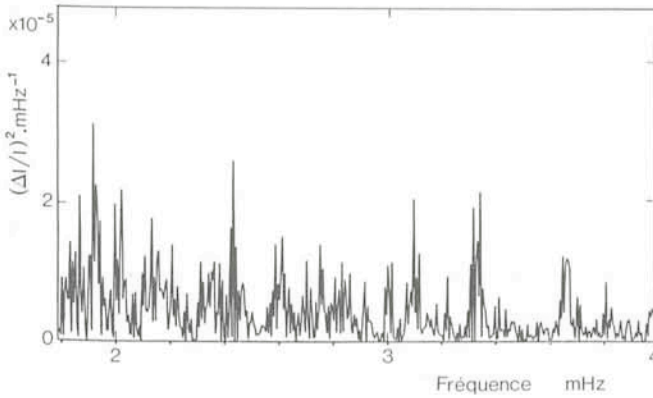


Fig. 1: Part of the power spectrum of the data consisting in the monochromatic intensity in the red wings of the Alpha Centauri A Na D lines, recorded during three consecutive nights (May 1983) at the Cassegrain focus of the ESO 3.6 m telescope.

– A reference channel, which contains the whole 20 Å pass-band of the interference prefilter.

The first step of the analysis consists in dividing the monochromatic intensity by the reference signal, in order to minimize the effect of atmospheric transparency fluctuations. This has proved to be sufficient in the presence of clouds, absorbing as much as 60% of the light. With thicker clouds, the diffusion of the moonlight makes the division inaccurate.

A harmonic analysis is then performed by Fourier analysis, whereby the whole data set is regarded as one single time series, including zeroes when data are not available. Fig. 1 shows the resulting power spectrum in the five-minute range where spectral peaks are looked for. Having the solar result in mind, we are looking for a set of equidistant peaks representing the resolution of alternatively even and odd degree eigenmodes. This power spectrum is evidently much noisier than the corresponding solar one (Grec et al., 1983). However, a regular pattern of about 80 μHz seems to be present just around 3 mHz. In order to check the significance of this possible pattern, the next step consists in looking for a periodicity by calculating the power spectrum of a given section of this power spectrum. This has the dimension of the

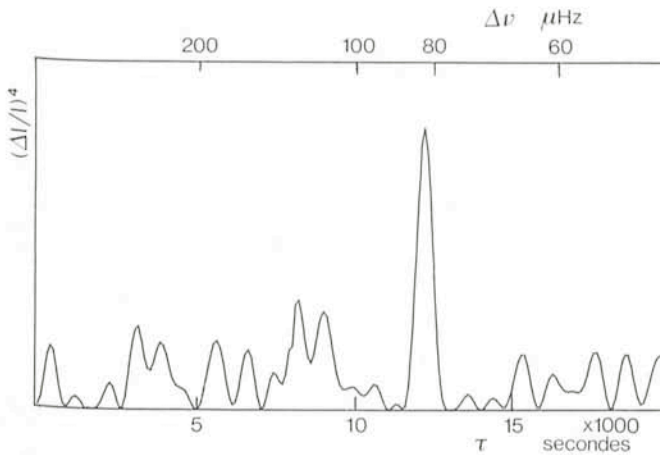


Fig. 2: Power spectrum of the power spectrum limited to the frequency range 2.3–3.85 mHz, corrected of the square of the window function autocorrelation. The major peak, at 81.3 μHz, means that the expected periodicity in the signal spectrum is indeed present.

square of an autocorrelation and therefore, the result shown in Fig. 2 has been corrected of the square of the autocorrelation of the temporal observing window. It shows convincingly that only one periodicity is present in the range 2.3–3.8 mHz of the power spectrum, with a period of 81.3 μHz.

Although significantly different, this result is of the same order of magnitude as the 68 μHz obtained in the solar case. It is then to be regarded as a very convincing evidence for the detection of five-minute p-modes on Alpha Centauri.

Now, once admitted the existence of a pattern of equidistant peaks in the power spectrum, the data analysis can be pursued one step further by trying to extract this pattern from noise. This is done by using the knowledge of the periodicity (81.3 μHz) and phase of this period provided by the Fourier analysis whose result is displayed in Fig. 2. An adapted filtering with this period and this phase is made on the power spectrum of Fig. 1 and with a resolution of 0.32 mHz (Sinus fitting at locked phase on 0.32 mHz wide slices of the power spectrum). The result, shown in Fig. 3, is compared to the envelope of the solar spectrum obtained with the same resolution (from Fossat et al., 1978). The similarity is really striking and does not leave any room for doubt about the significance of the result obtained on Alpha Centauri.

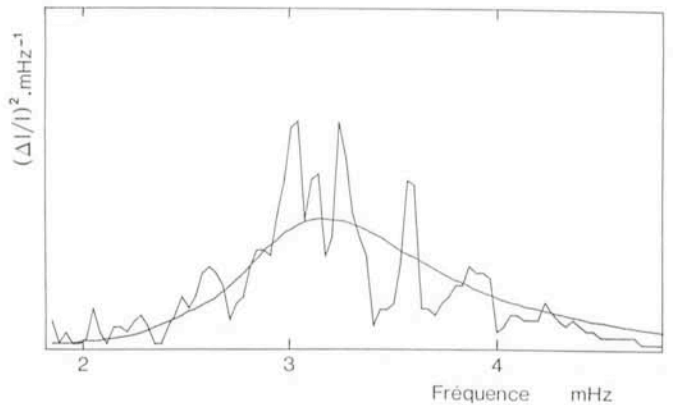


Fig. 3: Using an adapted filtering, locked in frequency and phase, it is possible to extract from surrounding noise the power contained in the discrete pattern which is present in the power spectrum of Fig. 1 (black part). The continuous line shows, for comparison, the same envelope measured with an identically resolved solar power spectrum.

Theoretical implications of this result must now be investigated. At first order, one can probably say that if the five minute p-modes are convectively excited, the close similarity of the two curves in Fig. 3 indicates that Alpha Centauri and the sun have presumably almost identical external layers, as their identical spectral type suggests. However, the frequency spacing within this envelope is significantly different. This spacing being directly related to the inverse of a sound wave travel time from centre to surface, the two stars are certainly notably different in their deeper layers. The sound travels faster in Alpha Centauri, which has then to be denser than the sun. Also, in the same frequency range, the radial order of excited eigenmodes is slightly smaller in the case of Alpha Centauri. For example, the major peak at about 3.3 mHz can be tentatively attributed to a $n = 19, l = 0$ or 1 mode while in the solar spectrum this is the frequency of the radial $n = 23$ mode.

We hope to obtain more data during the next observing runs, in order to resolve the pairs of odd and even peaks, like in the solar case.

References

- Claverie, A., Isaak, G.R., McLeod, C.P., Van der Raay, H.E., Palle, P.L., and Roca Cortes, T. 1984, Proceedings of the EPS Catania Conference.
- Deubner, F.L. 1975 *Astron. Astrophys.* **44**, 371.
- Fossat, E., Decanini, Y. and Grec, G. 1982, *Instrumentation for*

- Astronomy with large telescopes*, C. Humphries, ed. September 1981.
- Fossat, E., Decanini, Y., and Grec, G. 1983, *The Messenger*, **33**, 29.
- Gough, D.O. 1984, preprint.
- Grec, G., Fossat, E. and Pomerantz, M. 1983, *Solar Phys.* **82**, 55.
- Leighton, R. 1960, IAU Symposium n° 12 (Nuovo Cimento Suppl. 22, 1961).

A Close Look at Our Closest Neighbor: High Resolution Spectroscopy of Alpha Centauri

D. R. Soderblom, Harvard-Smithsonian Center for Astrophysics, Cambridge MA, USA

As most astronomers will tell you, most of the telescopes are in the northern hemisphere, and most of the interesting objects are in the south. The Magellanic Clouds, the largest globular clusters, and the center of our Galaxy are among the celestial objects that must be studied from south of the equator. Also in the deep south are the Sun's nearest neighbors – the α Centauri system. It contains three stars: (1) α Cen A has the same spectral type as the Sun, although it is slightly more massive; (2) α Cen B is a little less massive than the Sun and orbits α Cen A with a period of 80 years; and (3) Proxima Cen is a very low mass star that is slightly closer to us than either of the other two. Proxima Cen is moving through space in the same direction and at the same rate as α Cen A and B, but is very distant from them.

None of these three stars is particularly unusual – they certainly show none of the bizarre behavior of some astronomical objects. But it is their very ordinariness that makes them so interesting. Here are assembled three excellent examples of the lower main sequence, and they are much brighter than most stars, hence easier to observe. These stars, particularly α Cen A, bear a striking resemblance to our Sun, and so we naturally want to study them in great detail, in order to draw comparisons.

New astronomical instruments are designed to reach new frontiers. This often means being able to examine extremely faint objects at the edges of our Galaxy or the universe. But there is also an inward-facing frontier to be breached, a frontier in the quality of data for bright objects. Astronomical spectroscopy has traditionally used (and still does) photographic plates to record stellar spectra. Photographic emulsions are inefficient (only 1 in 1,000 photons gets recorded), and even for the best cases the data are mediocre. The quality of a spectrogram is measured by its signal-to-noise (S/N) ratio. An exposure with S/N = 100 means that there are random fluctuations of $\pm 1\%$ in the data. Such fluctuations prevent the detection of very weak absorption lines, and stronger lines do not get defined well enough to detect subtle but interesting phenomena. Photographic spectra rarely exceed a S/N of 100.

Technological advances in the last decade have produced the Reticon and the CCD. The Reticon is particularly well suited for high S/N spectroscopy of bright stars. It is better than 90% efficient at many wavelengths – hardly any photons are wasted! A Reticon is capable of producing data with S/N $\geq 10^4$. Obtaining such data is time consuming and difficult, but the efforts are rewarded by spectra of unprecedented detail.

Such a Reticon is in use on ESO's Coudé Echelle Spectrometer (CES), a high resolution stellar spectrograph that is fed by the Coudé Auxiliary Telescope (CAT). The CES is the best instrument of its kind in the southern hemisphere – no other

can deliver the same combination of high S/N and high spectral resolution. Because it is unique, ESO has granted time on the CAT/CES to North American astronomers; indeed, one such person was involved with the design and testing of the instrument. Further, our National Science Foundation provides travel funds to use such instruments if they do not duplicate US facilities.

I therefore found myself on La Silla in April 1983, using the CAT/CES to observe α Centauri A and B. My objective was to compare these stars to the Sun in order to learn about several age-related properties of solar-type stars. All of these properties relate to the presence of a convective envelope. Convection mixes the surface material deep down into the star. One manifestation of this mixing is that lithium atoms are gradually destroyed because they undergo nuclear reactions at a temperature of about two millions degrees. Although the exact process is poorly understood, the convective envelopes of solar-type stars must reach such a temperature because we can see that their lithium is depleted. For example, meteoritic material contains about 200 times the lithium that is now present on the solar surface, and very young stars also have lots of lithium. Old stars have little or no lithium. Because of this gradual lithium depletion, a star's lithium abundance can be used to estimate its age.

Determining a star's lithium abundance is difficult. If one wished to observe, say, iron in a star, there are hundreds of absorption lines to measure, and so some of the errors of measurement cancel out. But there is only one lithium feature available, at 6708 Å wavelength. To make matters worse, no element in the Sun is less abundant than lithium (except for the heavy, radioactive elements). The only positive factor is that this lithium feature is well out in the red, where modern detectors like the Reticon are especially sensitive, and where other spectral lines are less of a problem.

The solar lithium feature is extremely weak, and because of this some observers have claimed that it is not even there at all. However, some observations of extraordinary quality, made about ten years ago at Kitt Peak, provide an accurate solar lithium abundance. The Sun is the only old star for which a good lithium abundance exists, and is therefore crucial for calibrating the lithium abundance-age relation. Therefore α Cen A provides a good test of whether or not the Sun has a lithium abundance that is typical for a star of its mass and age.

To see why this is so, we need to consider the age of the Sun and α Cen. We know the Sun's age by radioactive dating of solar system material. We can also use stellar structure theory to calculate what the present properties of the Sun *ought* to be, and then compare those to the real Sun. As the Sun has grown older, it has converted hydrogen into helium in its core – this produces the solar luminosity. The very center of the Sun

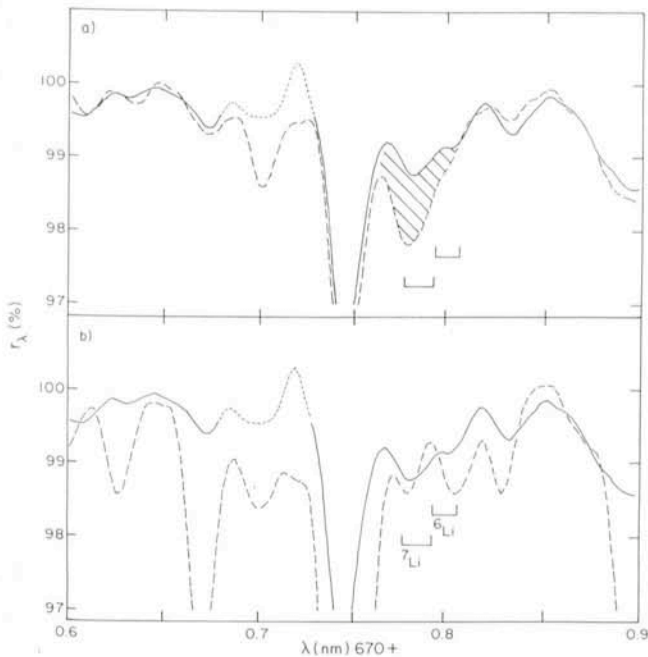


Fig. 1: Data from the CAT/CES for lithium in α Centauri and the Sun. Note the vertical scale: only the top three percent of the spectrum is displayed. In both panels, the solid line shows a solar spectrum (the dotted section is a Reticon imperfection). Panel a) compares α Cen A to the Sun, while b) shows α Cen B. The expected wavelengths of the lithium lines are shown in the lower panel. ${}^6\text{Li}$ is rare – it constitutes less than 10% of the total solar or terrestrial lithium. The ${}^7\text{Li}$ feature is a doublet, with the blueward component being twice as strong as the redward one. The shaded region in the upper panel shows the extra lithium absorption in α Cen A compared to the Sun.

gradually runs out of hydrogen, and this causes the structure of the Sun to adjust in order to keep the nuclear reactions going. Because of all this, the Sun has grown a little warmer and larger over its main sequence lifetime.

We can use the same theory to determine the age of α Cen. The parallax and apparent magnitude together define the star's true luminosity. Determination of the temperature is then needed to get the age, since we know the mass (because it is a

binary). This sounds straightforward, but is in reality difficult and uncertain. Because α Cen is in the south, it has not been as thoroughly observed as nearby stars that are in the north. Therefore the parallax and masses are not as well determined as we would like. The age one calculates depends on the composition of the star, and that is not known very well either. The best present estimates place α Cen at about 6 billion years old, just a little older than the Sun's 4.6 billion years.

For the purpose of understanding the lithium, it is sufficient to just compare α Cen A to the Sun. A great deal of effort is saved because it appears that they have the same temperature. Carefully determined spectral types for α Cen A and the Sun are identical. Comparing the spectra does not suffer from the usual problems of comparing the Sun to other stars: an excess of light that stellar equipment cannot handle. Another way of comparing temperatures is to compare $\text{H}\alpha$ profiles. Again, α Cen A and the Sun appear to be indistinguishable.

If we assume that α Cen A and the Sun have exactly the same temperature, getting a lithium abundance is easy; we just need good measurements of the line strengths. An example of the lithium spectral region is shown in Fig. 1. You can see that the lithium spectral feature is a good deal stronger in α Cen A than it is in the Sun, but lithium is probably absent from α Cen B. These data indicate that α Cen A has about twice the solar lithium abundance. D. Dravins of Lund Observatory has also observed lithium in these stars, during the commissioning of the CAT/CES, and his data give the same result.

What does this mean? Remember that α Cen A is slightly more massive than the Sun (10% more), while α Cen B is 9% less massive. The depth of the convective envelope is extremely sensitive to a star's mass, so α Cen A should have a thinner convective zone than the Sun does. Therefore the lithium depletion will be slower, and α Cen A's greater lithium abundance is reasonable. Similarly, a star like α Cen B depletes lithium much faster than the Sun does, and it has none left.

There are other age-related properties that are being studied in these stars, such as the strength of their chromospheres and their rotation rates. They will have to be discussed another time.

The staff of ESO make observing there a real pleasure. I would particularly like to thank Sr. José Véliz for his help.

Ca II in HD 190073 Revisited

A. E. Ringuet, Instituto de Astronomía, Buenos Aires, Argentina, and
J. Sahade, Instituto Argentino de Radioastronomía, Villa Elisa, Argentina

In 1933, Paul W. Merrill, of the Mount Wilson Observatory, published, with the collaboration of Cora Burwell (Merrill and Burwell, 1933), a Catalogue of such attractive objects as the B and A stars that display emission lines in their spectra.

The classical model for the Be stars suggests that we are dealing with evolved (off the main sequence) objects and that the emission arises because of a geometrical effect in the flat, extended envelope that surrounds them. This envelope would result from the shedding of matter through the equatorial bulge because of instability generated by the large rotational velocities that seemed to characterize our group of objects. Such a model is, however, vulnerable in many aspects, as recent studies, particularly those that cover the satellite ultraviolet

wavelength region, have disclosed. Indeed, the apparent correlation of rotational velocity and emission is no longer an established fact, the mass loss rate does not seem to be related with velocity of rotation, and it does not seem to be necessarily true that the emission is observed because of a geometrical effect. The investigation of Be and Ae stars, in as an extended a wavelength range as possible is, therefore, most desirable if we wish to reach a full understanding of their nature and of the structure and extent of their gaseous envelope.

One of the particularly interesting stars of the group is the one listed under number 325 in Merrill and Burwell's (or Mount Wilson) Catalogue and known as MWC 325, or, more gener-

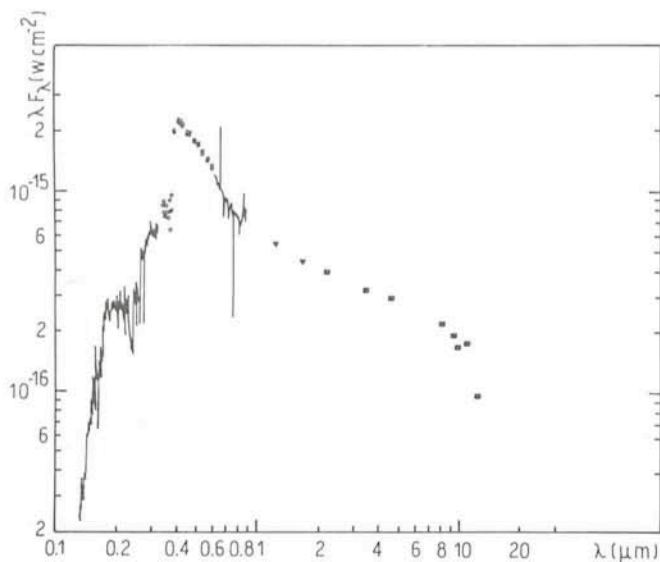


Fig. 1: Energy distribution of HD 190073 (from Saitko et al., 1981).

ally, as HD 190073, for its number in the *Henry Draper Catalogue*. The star is in the constellation of Aquila.

In their "Notes to the Catalogue", Merrill and Burwell pointed out that HD 190073, an A0 object, is characterized by a "most peculiar spectrum" where "the sodium $D_{1,2}$ lines are bright, and the structure of the H and K lines [of Ca II] are very remarkable". The discovery that the star's spectrum shows $H\alpha$ in emission was made by Merrill in 1927, who also discovered a few years later the structure in Ca II.

HD 190073 is also characterized by the presence of a magnetic field. H.W. Babcock (1958) found that different elements or ions yielded different field intensities and polarity, namely,

Cr I, Fe I:	+ 270 ± 30 gauss
Si II:	+ 120 ± 30
Fe II, Ti II, Cr II:	+ 5 ± 30
Mg I:	0
Ca II:	- 270 ± 30

and it may be significant that neutral metals yield larger field intensity than ionized metals, and that Ca II suggests a different polarity.

Another interesting feature of our star is that it has a large infrared excess, as was reported by S.L. Geisel (1970). Woolf, Stein and Strittmatter (1970) have shown that, in some cases, infrared excesses in Be stars can be accounted for by free-free radiation from an ionized hydrogen envelope with an electron temperature of the order of 10,000° K. In HD 190073 the infrared excess ($H-K = 0.79$ mag. and $K-I = 1.20$ mag.) cannot be understood purely in terms of Woolf et al.'s model. D.A. Allen (1973) suggests that in HD 190073 the infrared excess arises principally from thermal emission from grains in a circumstellar dust shell of a temperature little above 1,000° K that surrounds the object, and, in his paper on the "near infrared magnitudes of 248 early-type emission-line stars and related objects", illustrates eight cases of Be and Ae stars for which the infrared excesses can be similarly explained. An alternative—we should perhaps say, complementary—model of free-free emission from HII regions around the stars, where the electron temperatures are of the order of $1-8 \times 10^3$ K, has been proposed by Dyck and Milkey (1972). Actually, the flux from HD 190073 in the infrared suggests that we probably have contributions from an HII region, from an HI region and from a dust shell.

Fig. 1 depicts the energy distribution of HD 190073 from the IUE shortest UV wavelength through the infrared, as compiled by Sitko, Savage and Meade (1981). We can readily see that the energy distribution departs from a normal one.

In order to try to make a contribution towards a better understanding of the peculiar spectrum of the star, in particular of the structure in the lines of Ca II-H and K, in August 1982, we observed HD 190073 at La Silla with the coude spectrograph of the 1.5 m telescope, in the blue, with a dispersion of about 12 \AA mm^{-1} , and in the red region of the spectrum, the latter with a dispersion of about 20 \AA mm^{-1} . The La Silla material was supplemented with IUE high dispersion images that existed in the NASA Goddard Space Flight Center archives and were partially studied by one of us (J.S.) with the use of the IUE RDAF (Regional Data Analysis Facility) in June–July 1983.

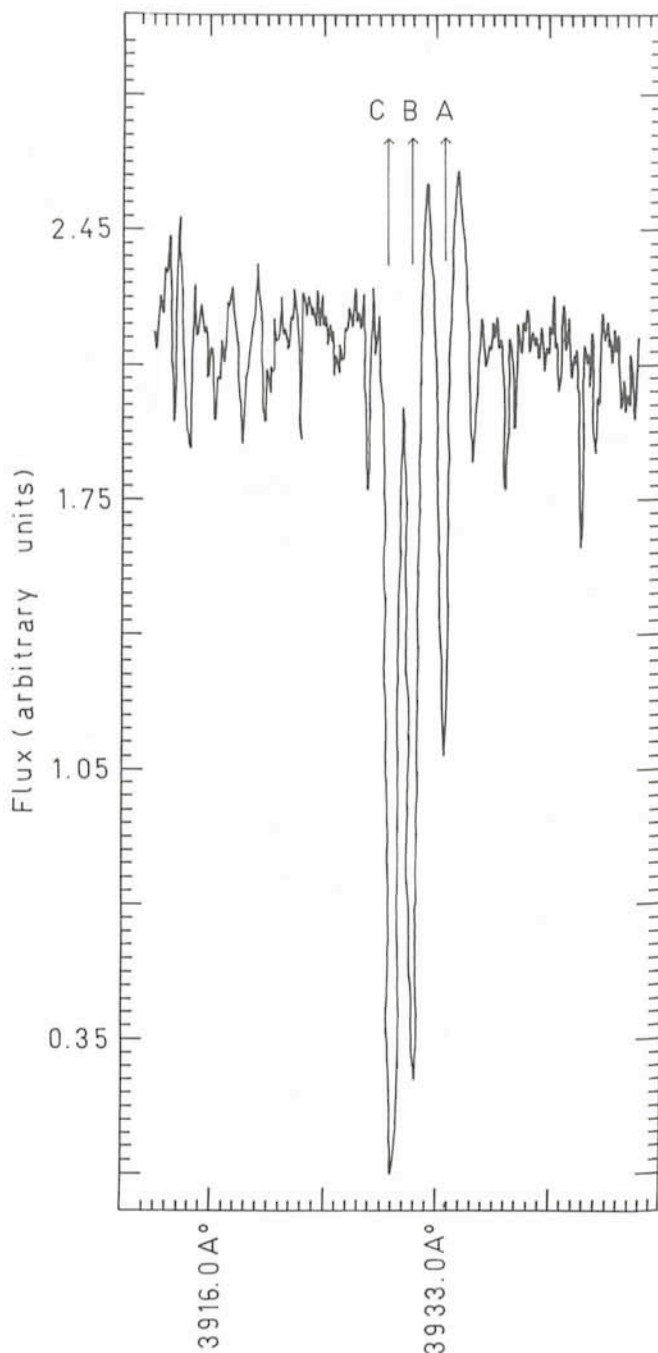


Fig. 2: The profile of Ca II-K, from a spectrogram taken by the authors at La Silla.

The spectrum of HD 190073 is most interesting and a detailed discussion of our results will be published in a professional journal. Here we would like to confine ourselves to the description and discussion of the profiles of the Ca II lines.

Fig. 2 illustrates the profile of the K line of Ca II at 3933.7 Å. We distinguish, going from shorter to longer wavelength, two narrow and deep absorptions (C and B on the figure, following Merrill's nomenclature) and an emission feature with a narrow and fairly deep absorption feature superimposed (A on the figure, following Merrill's nomenclature). Exactly the same is true for the Ca II-H line at 3968.5 Å.

Naturally, being so peculiar, the Ca II profiles have been extensively studied since their discovery, and some facts have been established. In the first place, Merrill was able to ascertain the constancy of the presence of the three strong and narrow absorptions A, B and C, and also the fact that, at times, components B and C are not single but display several subcomponents. More recently, J. Surdej and J.-P. Swings (1976, 1977) secured further observations and analyzed the spectra taken of the star during the interval of over 30 years, from 1943 through 1974. This work confirmed Merrill's conclusions and further disclosed that "the details of the H- and K-complex structure are correlated with the profiles of the Balmer lines".

On the observations we secured in 1982, we find the permanent absorption structure—and the emission—in the Ca II profiles, with no subcomponents. The derived radial velocities are 0, -180 and -300 km s⁻¹ for components A, B and C, respectively.

Now a question arises. Are there lines of other elements or ions in the spectrum of HD 190073 that display the same profile as Ca II, or, at least, yield radial velocities of the same order as those derived from the absorption components in the profile of Ca II? An affirmative answer comes from the study of the material at our disposal.

On the spectra taken at La Silla, if we look at the Fe II lines that have stronger emissions, namely, those of multiplet 42, at 4924, 5018 and 5169 Å, we find that the line at 4924 Å displays a similar structure as Ca II. This is illustrated in Fig. 3, where we can see emission at about the normal position of the line, and absorptions A, B and C, yielding radial velocities of 0, -207 and -295 km s⁻¹, respectively, plus an additional absorption between A and B, which we have called D in Fig. 3 and yields a radial velocity of -110 km s⁻¹. The line at 5018 Å does not show component C, and, at 5169 Å, component C is perhaps very weakly present. The Fe II lines of multiplet 42 display an additional feature, namely a sort of a bulge at the violet edge of the emission, which we will not discuss here.

The similarity in profile of the lines of Ca II and Fe II (42) and in the radial velocities of the common features suggest that perhaps these components of Ca II and Fe II are formed in the same regions of the gaseous envelope that surrounds the star. The question is as to whether we can say anything about the relative position of such regions. But before we try to take up this question let us add information from the IUE ultraviolet spectrum, of which we have, so far, analyzed only a few selected regions.

The IUE ultraviolet spectrum of HD 190073 displays only absorption features, except in the case of the resonance lines of Mg II at about 2800 Å, and is rich in Fe II lines, which are single and violet-displaced in the velocity interval -210 ± 35 km s⁻¹. The ultraviolet Fe II lines appear, therefore, to coincide with what we have called component B of Ca II and of Fe II (42) on the ground-based spectra. As a consequence, the first conclusion we can draw is that component B of Ca II and Fe II, which is devoid of emission, should form in a region located not too far from the stellar surface, and that component A,

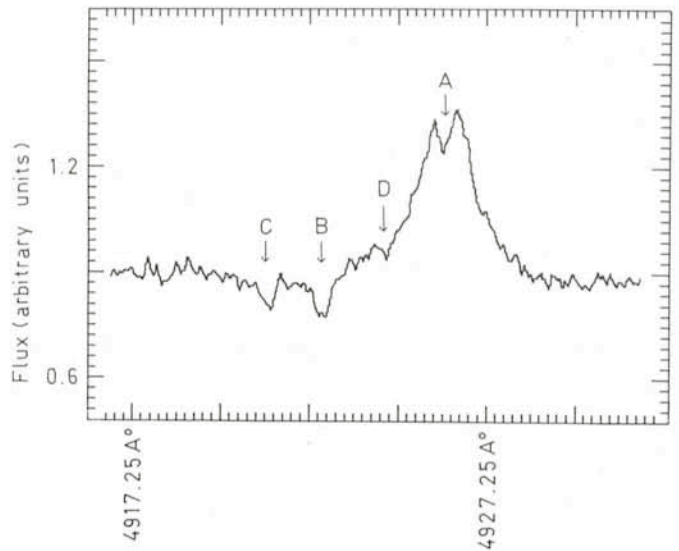


Fig. 3: The profile of Fe II at 4924 Å, from a spectrogram taken by the authors at La Silla.

which is associated with emission, should arise farther away, at a certain distance from the star. The latter assertion is supported by the fact that Na I displays a profile that, in all respects, is similar to that of component A and the associated emission.

Then, the subcomponents connected to component B that are observed at times, indicate that some kind of activity takes place close to the star. This conclusion, which finds further support in the similar conclusion that was reached in a recent study that we have carried out, jointly with other investigators, of the Be star V 923 Aquilae (Ringuet et al., 1984), contributes to our knowledge and a better understanding of emission-line B and A stars.

Regarding component C, that, at times, also displays subcomponents and is devoid of emission, we can only say at present that the region of formation should be relatively close to the star, and should undergo variations in the local conditions with a time scale that could be, according to Surdej and Swings, even of the order of hours.

A complete analysis of the spectrum of HD 190073, in the photographic as well as in the satellite ultraviolet regions—which is near completion—and its possible interpretation in terms of a theoretical model, may improve our picture of the gaseous envelope around the star. The presence of the resonance lines of Si IV and of C IV in the IUE spectrum, that suggests the existence of a "transition region" in the envelope, and the information regarding the star's magnetic field are two important items that should then be taken into consideration.

Acknowledgements

We are indebted to Mrs. Margarita Trotz for very kindly preparing the illustrations for this article.

The work of one of us (J.S.) was partly supported by Computer Sciences Corporation through a sub-contract under NASA Contract NAS 5-25774.

References

- Allen, D.A.: 1973, *Monthly Notices Royal Astronomical Society* **161**, 145.
- Babcock, H.W.: 1958, *Astrophysical Journal Supplement* **3**, No. 30.

Dyck, H.M. and Milkey, R.W.: 1972, *Publications Astronomical Society of the Pacific* **84**, 597.
 Geisel, S.L.: 1970, *Astrophysical Journal Letters* **161**, L 105.
 Merrill, P.W. and Burwell, C.G.: 1933, *Astrophysical Journal* **78**, 87.
 Ringuelet, A.E., Sahade, J., Rovira, M., Fontenla, J.M. and Kondo, Y.: 1984, *Astronomy and Astrophysics* **131**, 9.
 Sitko, M.L., Savage, B.D., and Meade, M.R.: 1981, *Astrophysical*

Journal **247**, 1024.
 Surdej, J., and Swings, J.-P.: 1976, *Astronomy and Astrophysics* **47**, 113.
 Surdej, J., and Swings, J.-P.: 1977, *Astronomy and Astrophysics* **54**, 219.
 Woolf, N.J., Stein, W.A., and Strittmatter, P.A.: 1970, *Astronomy and Astrophysics* **9**, 252.

Determination of the Rotation Curve of Our Galaxy. Observations of Distant Nebulae

J. Brand, Sterrewacht Leiden, Netherlands

For the derivation of the Galactic gravitational potential, a well calibrated rotation curve of a suitably selected class of objects is a valuable source of information. It gives us insight in problems of galactic dynamics and mass distribution.

This article describes the project currently carried out by the author, in collaboration with Dr. Jan Wouterloot (formerly with ESO) and Dr. Leo Blitz (University of Maryland). Its main purpose is to determine the shape and strength of the gravitational force that influences the motion of material in our Galaxy. We do this by turning our attention to the outer galaxy (third and fourth quadrant), where we try to figure out how the molecular material, and by inference the (young) stars that reside in the disk, moves in those outer reaches of our stellar system. Knowledge of the gravitational potential will give us insight in the way mass is distributed in the Galaxy.

The fact that the Galaxy rotates has been established by Lindblad and Oort in the mid 1920s. The rotation is differential, i.e. the Galaxy does not rotate as a solid disk (as for instance do the wheels of a car, fortunately), but has a different angular velocity at different distances R from the galactic centre (G.C.). Furthermore it is found that different types of objects move in different ways, in the sense that the gas is constrained to move in nearly circular orbits around the G.C., whereas old stars (members of the so-called spheroidal component) move in highly eccentric orbits. The relation that gives the velocity of rotation in circular orbits with respect to the G.C. as a function of distance from the G.C. is called the rotation curve. Ever since the 1920s people have been trying to determine the rotation curve of our galaxy. There are several reasons why this relation is important. Matter in the Galaxy is distributed in a certain way, which determines the shape of the gravitational potential. This potential dictates the orbital parameters of the galactic constituents (stars and gas) and thus the rotation curve that we derive from our measurements of these constituents. Reversing the sequence, the rotation curve tells us how matter in the Galaxy moves and gives clues as to how it is distributed. A practical, and very important, use of a rotation curve is to estimate distances to gas clouds (either HI or HII regions for which the ionizing stars are too much obscured to be seen) by just measuring their velocity.

There are several ways to determine the rotation curve of our Galaxy, depending on the sector of the Galaxy that one investigates. For the inner Galaxy ($l = 90^\circ \rightarrow 0^\circ \rightarrow 270^\circ$) a much used practice is to measure the velocity of the atomic or molecular gas (through respectively the 21 cm line of HI or the 115 GHz (or 230 GHz) line of CO). For a particular line of sight, the emission of the highest-velocity feature is then assigned to the location closest to the G.C., encountered along that line of sight. In this way a rotation curve for the part of the Galaxy inside the solar circle can be constructed. Another way to

reach this goal is to use HII regions and their exciting stars. In that case, the velocities used are that of the ionized gas (e.g. via H α , or H109 α line measurements), of the stars (thought to be) associated with the nebulae, or of the molecular clouds associated with the HII regions. Distances are derived from optical observations (photometry and spectrography) of the exciting stars. Other galactic objects such as Cepheids and planetary nebulae can and have been used as well. From that combined work we now have a fairly good understanding of the rotation characteristics of the inner Milky Way. A disadvantage encountered in the inner Galaxy is that the line of sight samples each radius R twice. This situation is depicted in Fig. 1. Measuring a radial velocity of an object in that part of the Galaxy leaves one in doubt as to whether to assign it to the "near" or "far" distance. One then has to use circumstantial evidence (such as degree of extinction for HII regions or angular sizes of gas clouds in the direction perpendicular to the galactic plane) to solve this dilemma.

For the outer Galaxy ($l = 90^\circ \rightarrow 180^\circ \rightarrow 270^\circ$) things are more straightforward as each velocity corresponds directly to

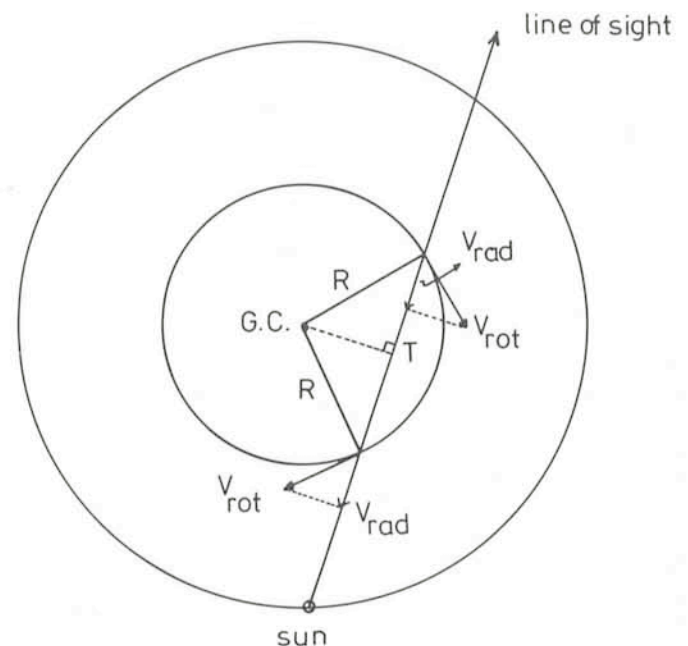


Fig. 1: Distance ambiguity in the inner Galaxy. The line of sight intersects the circle that is the locus of points at a distance R from the G.C. twice. Objects at both intersections have the same velocity. It is assumed that the highest-velocity features along this line of sight are found at point T (= tangential point). V_{rot} and V_{rad} are rotational and radial velocity respectively.

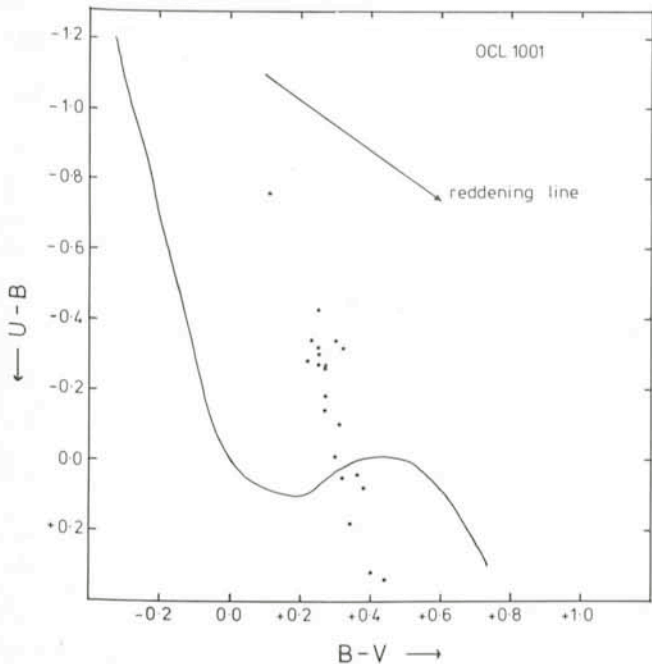


Fig. 2: Colour-colour diagram of the open cluster OCL 1001, constructed from UBV observations with the ESO 1 m telescope. All plotted stars are cluster members. Due to little internal reddening, the points form a sequence parallel to the unreddened ZAMS (drawn curve). The unreddened colours are found by shifting the data points along the reddening line to the ZAMS.

a single distance. There are some other advantages as well, not the least of which is that it is visible from La Silla. In that part of the Galaxy, one can still use H II regions and associated stars and gas to derive the rotation curve. We use the H II itself only as a tracer. It guides us to the stars that we measure to find their distances, and it tells us where the molecular material (invisible to the eye), of which we measure the radial velocity, is to be found. CO surveys have shown that there is not much molecular gas outside the solar circle, so there will be fewer identification problems as to which H II region is associated with which cloud, especially at velocities appreciably different from zero. And finally, related to this, there is a smaller amount of extinction in those parts of the Galaxy than there is in the inner Galaxy, so that we can expect to see quite far out.

The basis of our project are the 600 odd emission objects identified by the author from ESO/SRC survey plates in the region $230^\circ \leq l \leq 305^\circ$, $|b| \leq 10^\circ$. These are either H II regions or reflection nebulae (both types of objects can be used). From the plates we have tried to identify those stars that are likely to be associated with the nebulae (by looking at their position relative to a nebula and signs of interaction, such as bright rims). The first step is then to obtain photometry of those stars. For this we have used the Walraven VBLUW photometer at the Dutch 90 cm and the UBV photometer at the ESO 1 m telescope.

If we plot the colours of the stars of a particular region in a colour-colour diagram (e.g. U-B vs. B-V) and then shift them back, along the reddening line, to the unreddened ZAMS* in that diagram, we obtain the unreddened colours of that star $((U-B)_0$ and $(B-V)_0$) and the colour excess $E(B-V) = (B-V) - (B-V)_0$. From the colours we get an absolute magnitude M_V and from the colour excess we find the visual extinction $A_V = R \times$

* The ZAMS (Zero Age Main Sequence) is the locus of points in the colour-colour diagram on which a star lies at the beginning of its evolution, at the onset of H burning.

$E(B-V)$ ($R \sim 3.2$). We can then derive the stars' heliocentric distance d through the well-known relation $V - M_V = 5 \log d - 5 + A_V$. Using simple geometry, heliocentric distance is converted into galactocentric distance R . When all stars selected are in fact associated with the emission nebula, shifting each star individually will result in the same distance (allowing for some intrinsic spread). Furthermore, if there is no or very little internal reddening in the group, the stars will form a sequence in the colour-colour diagram parallel to the unreddened sequence. This is nicely illustrated in Fig. 2, which gives the observational data of the open cluster OCL 1001 plotted in the (U-B) vs. (B-V) diagram, together with the unreddened ZAMS relation. However, the case is much less clearcut for other objects. This is mostly due to the fact that it is hard to identify possibly associated stars for an H II region so that only some of the selected stars will actually excite the emission region in question. Plotting the data in a colour-colour diagram then gives anything but a nice sequence. This is furthermore complicated by the fact that only stars of luminosity class V should be shifted back to the ZAMS, since stars of other luminosity classes (e.g. Ia (supergiants) or III (giants)) have different unreddened sequences in the diagram. Therefore, knowledge of luminosity class is important. If it is not known, it is relatively safe to assume a luminosity class V for an ionizing star, but a discrepancy in distance between two stars thought to be associated with the same emission region can mean that at least one of the stars is in fact not associated or has a different luminosity class. Therefore, spectra of stars will be taken as well (when this article was written, these observations still had to be done). To illustrate how well this method can work in case we do have knowledge of the luminosity class of the stars, and to show that the distances found are consistent with earlier findings, we have compared in Fig. 3 heliocentric distances derived from the VBLUW data in the way described above, using the published luminosity class, with distances

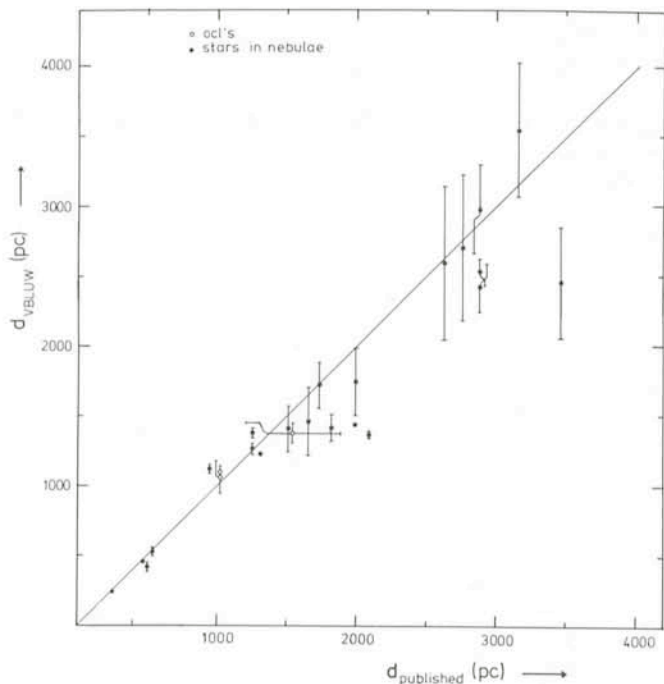


Fig. 3: Comparison of heliocentric distances determined from VBLUW photometry with published distances of the same objects. Plotted points are stars associated with nebulousity and open clusters (in the latter case, average distance of measured member stars is shown). Except for one OCL, no uncertainties are shown for published distances.

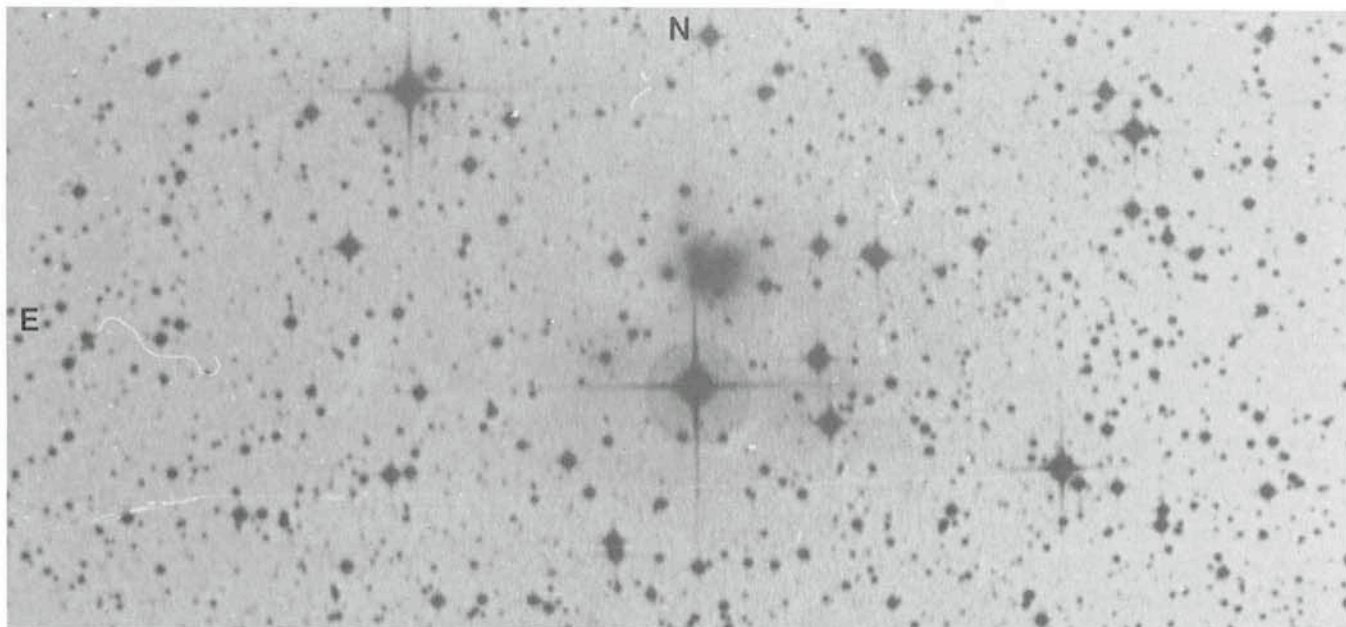


Fig. 4: Example of an emission region in our catalogue with easily identifiable associated stars. In the direction of this region we measure a velocity of 51 km s^{-1} for the CO line. The region is at galactic coordinates $l = 248^\circ$, $b = -5^\circ.5$. Photograph reproduced from ESO/SRC sky survey.

taken from the literature. As we measure five magnitudes in the Walraven system we can construct three independent colour-colour diagrams. The distances shown in Fig. 3 are an average derived from those diagrams.

So much for the way in which the distances are derived. How about the velocities? Half of our total sample of objects was observed with the CSIRO 4 metre dish (Epping, Australia) last year. The remainder will be done later this year. These observations have yielded interesting results in itself. For instance, some line profiles displayed quite broad wings indicating activity in the molecular cloud. Of more concern to the present project, about ten or fifteen clouds near nebulae showed up at velocities in excess of 50 km s^{-1} with respect to the local standard of rest. Examples of such regions are shown in Fig. 4 and 5. A crude indication of the importance of these regions can be given by taking the rotation curve that has been determined by Blitz and co-workers (Blitz, 1979) in similar fashion using the Sharpless H II regions in the second and part of the third quadrant, and substituting the measured radial velocity in a rotation curve equation to get its distance (which is one of the advantages of having a rotation curve at one's disposal, as the reader may recall). With a radial velocity of 77 km s^{-1} , region A of Fig. 5 would be at a distance $R \sim 17$ or 18 kpc from the G. C. From our work so far, and from work done by others in the second galactic quadrant, we infer that it is not very likely that we will find objects very much farther away than this. It seems that what an outside observer would call "the visible disk of the Galaxy" extends at most to about $R = 20 \text{ kpc}$. Even so, as we do not limit ourselves to previously catalogued (and usually relatively nearby) H II regions, we hope (and expect) to find many objects between $R = 15$ and 20 kpc , so that the rotation curve out to that limit can be well determined. Due to the large number of objects in our catalogue, for all of which we can, in principle, determine accurate distances, the errors in the rotation curve will be much smaller than those of previous projects. The stars we think are associated with the nebulae in Fig. 5 are hard to identify (for nebula A) and also too faint ($V \geq 17^m$ for nebula B) for photometry with either the Dutch or the ESO 1 metre telescope. We therefore observed this region (and others like it) with the CCD camera at the new 2.2 metre at La Silla, using B,

V and R filters. In this way we get colours of all stars in the $1'.7 \times 3'.0$ field of view, and down to faint magnitudes (as these data have only been gathered in February 1984, we have not yet been able to reduce them).

We hope to convey the results of our oncoming observing sessions to the reader in a future note to the *Messenger*.

Comments from Tim de Zeeuw and Frank Israel on an earlier version of the manuscript are appreciated.

Reference

Blitz, L., 1979, *Astroph. J. Lett.* **231**, L115.

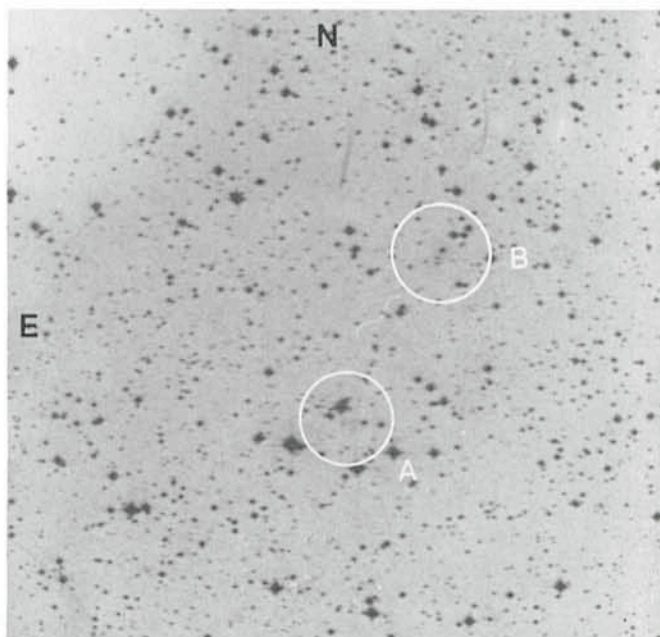


Fig. 5: Example of emission region in our catalogue, associated with molecular material having high radial velocity (reproduction from ESO/SRC sky survey). In the direction of A a CO line at a velocity of 77 km s^{-1} is detected. For B, a line at $V_{\text{LSR}} = 72 \text{ km s}^{-1}$ is measured. Regions A and B are at $l = 237^\circ$, $b = -1^\circ.3$.

Optical Haloes Around Galaxies

R. Beck, R.-J. Dettmar, R. Wielebinski, Max-Planck-Institut für Radioastronomie, Bonn, FRG
N. Loiseau, C. Martin, Instituto Argentino de Radioastronomía, Villa Elisa, Argentina
G.F.O. Schnur, Astronomisches Institut der Ruhr-Universität, Bochum, FRG

There are many reasons why massive haloes are expected to surround galaxies. Flat rotation curves are observed in spiral galaxies out to the largest observable distance from the nucleus. Studies of galaxies in pairs, groups and clusters also suggest mass at large distances from the galaxy centre. From these considerations the "missing mass" was postulated and various authors came with spectacular suggestions to explain this: small black holes, heavy leptons, neutrinos with rest mass, ordinary matter in particles of any size between gravel

and Jupiter. Could the missing mass be "hidden" as late type dwarf stars? Is there any indication for weakly luminous matter surrounding galaxies? Do we see reflection from dust in outer reaches of galaxies? How big are galaxies?

Answering all these questions is not easy. The light of a galaxy usually falls off very rapidly from the nucleus so that in the outer reaches of galaxies the light is usually well below the night sky level. Airglow variations (and the cirrus clouds) disturb the photometric measurements at distances from the

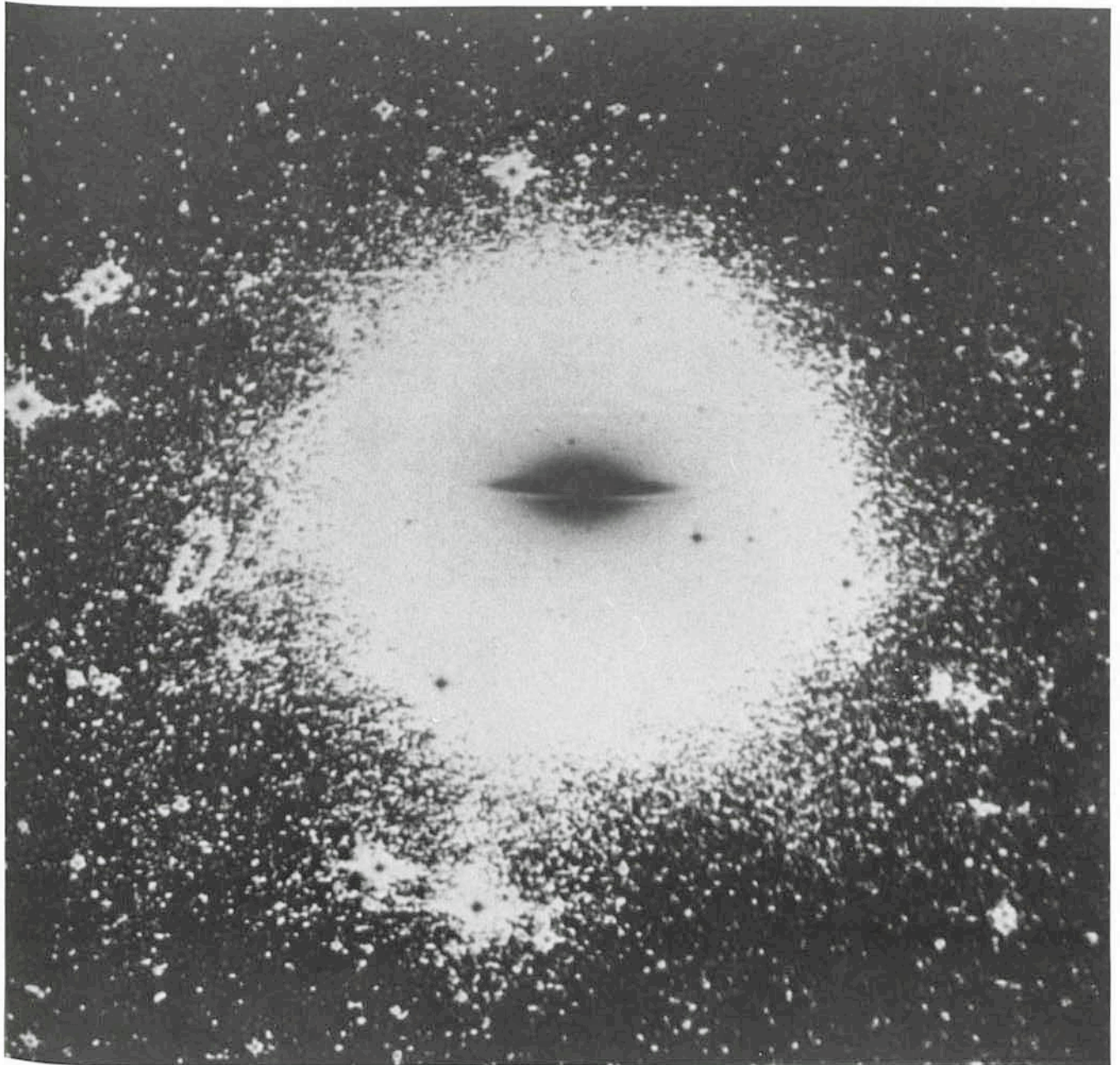


Fig. 1: The digitized image of M104 – the well-known Sombrero galaxy – from a deep IIIa-F plate of the ESO Schmidt telescope. North is at top, east to the left and the field shown is $\sim 34'$ on a side. The grey scale representation produces a pseudo-contour at a surface brightness of $\mu_R \cong 25 \text{ mag}/\square''$.

nucleus which are necessary to start to answer the many questions. However some pioneering work on selected edge-on galaxies (see review by Kormendy (1980)) showed that with modern techniques such studies are possible.

The rapid development of observing techniques has aided this type of work. The use of fine grain sensitized astronomical plates with subsequent diffuse light enhancement (e.g. Malin, 1978, 1981; Beck et al., 1982) allowed the study of the large nearby edge-on or nearly edge-on galaxies. Also the use of digitizing microdensitometers with subsequent data processing enables us to search for weak light. The CCD cameras now available are ideally suited for similar studies of smaller edge-on galaxies.

We have so far concentrated our attention on the large southern galaxies NGC 55, NGC 253, NGC 4594 (M104) and

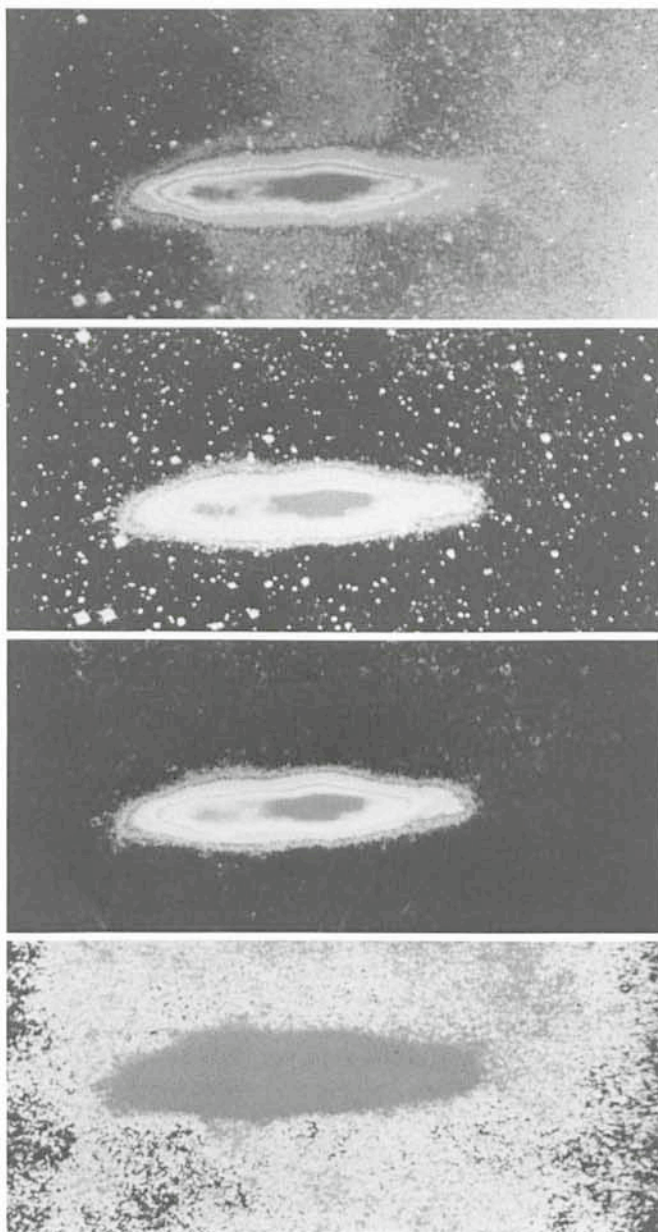


Fig. 2: The steps of reduction are demonstrated for NGC 55 which is a Magellanic type irregular galaxy of the Sculptor group seen edge-on. A large gradient in the background is visible in the field scanned from a standard SRC-J survey film. This gradient is corrected in the first step. In the second step foreground stars are removed. In the final step some smoothing shows a thick disk of weak light surrounding the galaxy.

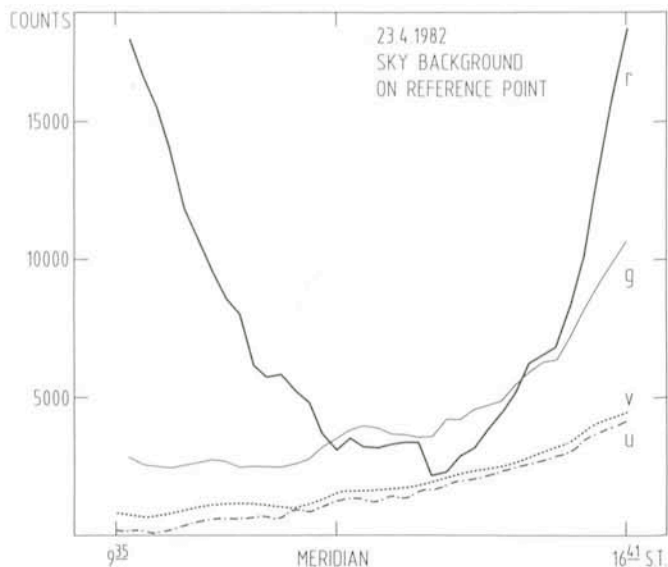


Fig. 3: Night sky variations during a 'good' night measured continuously at a reference point by the monitor telescope. The general trend is due to extinction but the spurious variations are comparable to the signal expected from a weak light surrounding a galaxy.

NGC 4945. Similar studies of a number of large northern edge-ons are planned. In addition to using the Schmidt plates we made photoelectric photometry measurements on selected points in the galaxy disk and in the halo. Also a number of surrounding stars were measured, so that the scanned plates can be "tied-in" to stellar images.

The Schmidt plates were taken in four colour ranges: U, B, R and I. The plates were all sensitized and exposed to the sky limit. It was the fine work of the Schmidt telescope staff that gave us the uniform plates. And a lot of this was done during the bad-weather period at La Silla! The plates were scanned with the PDS machines at ESO, Munich, and Münster University. The image processing was done on the VAX of the Astronomical Institutes of Bonn University. We used both the Starlink ASPIC and the MPI NOD software systems to present the data. One result, shown in Fig. 1, is the giant halo surrounding M104 which is seen after digitizing and computer processing. The photographic laboratory of the MPIfR also produced diffuse light pictures from the plates. The results were very similar, but the treatment of the digitized image with various filtering and convolving functions seems to offer the possibility of seeing more of the halo. Another example of a sequence of manipulations is shown in Fig. 2. Here we see the original plate, the plate with the large-scale gradient removed, the galaxy after filtering out of point-like objects (stars) and a weak-light enhanced version. This manipulation was made from a normal survey plate where the galaxy NGC 55 is taken nearly at the edge of a standard field.

The photoelectric photometry measurements were made on our galaxies with the 1 m and 50 cm ESO telescopes used simultaneously. We used the Thuan and Gunn (1974) uvgr filter system, because the passbands of this system avoid the strongest night sky lines. The two telescopes together allow us to monitor the night sky variations and achieve further reduction of these spurious signals. The most sensitive observations reached $\mu_B \approx 27 \text{ mag arcsec}^{-2}$. To make the observations, one astronomer from Bonn was joined by a partner from the Instituto Argentino de Radioastronomía, Villa Elisa, and the simultaneous observing was done via the telephone between the domes. Measurements of the sky brightness during a

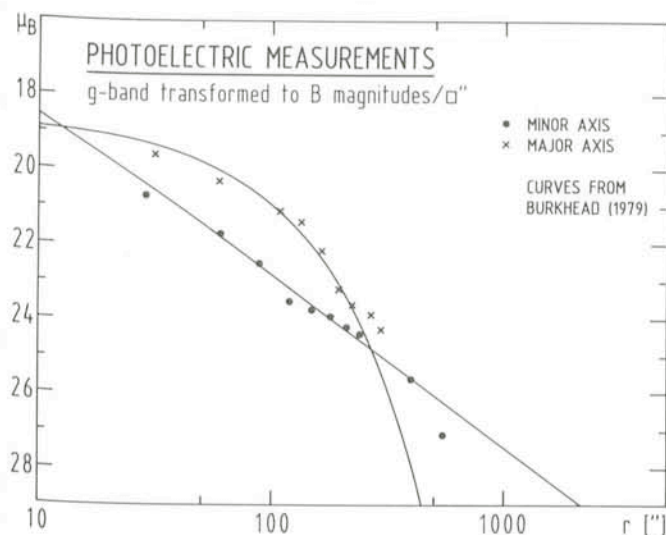


Fig. 4: The monitoring telescope technique allows photoelectric photometry down to a surface brightness of $\mu_v \sim 27 \text{ mag}/\square''$. Our photometry of M104 is compared with photographic photometry by Burkhead (1979). The g-band was transformed to B magnitudes assuming a colour of $B-V = 1.0$.

"good" night on La Silla are shown in Fig. 3. A bad night (70% of the nights in this project were bad) shows constant jumps of counts and cannot be used for the determination of the colour.

The galaxy NGC 4594 (M104) is the prime "standard" (Fig. 1) since it was known to possess an extended halo (Burkhead, 1979) and it can also be observed from northern sites. In Fig. 4 we show the results of our observations superimposed on the profiles derived by Burkhead (1979). The colour of the halo emission is red with $B-V \cong 1.0$. We found no significant variations of this colour out to the limits of detection in the halo of M104.

In studies of NGC 4565, Jensen and Thuan (1982) also find no definite colour gradient in the halo and $B-V = 0.9$. On the other hand, the colour of the halo surrounding NGC 253 is bluer.

The present sensitivity is such that we can study weak light in outer reaches of galaxies. The question of the origin of this light is still unclear. Lack of reliable colour information at the faint end of a galaxy makes it difficult to make any interpretations. Also the sample of galaxies that has so far been investigated is too small. Further studies using CCD detectors with colour and polarization filters are needed to bring us nearer to an interpretation of this very interesting phenomenon.

Acknowledgements

We thank H.E. Schuster and his staff for the Schmidt plates.

References

- Beck, R., Hutschenreiter, G., Wielebinski, R.: 1982, *Astron. Astrophys.* **106**, 112.
 Burkhead, M.S.: 1979, in *Photometry, Kinematics, Dynamics of Galaxies*, ed. Evans, University of Texas, p. 143.
 Jensen, E.B., Thuan, T.X.: 1982, *Astrophys. J. Suppl.* **50**, 421.
 Kormendy, J.: 1980, in *ESO Workshop on Two Dimensional Photometry*, eds. P. Crane and K. Kj ar, p. 191.
 Malin, D.F.: 1978, *Nature* **276**, 591.
 Malin, D.F.: 1981, *Sky and Telescope* **62**, 216.
 Thuan, Y., Gunn, J.E.: 1976, *Publ. Astron. Soc. Pacific* **88**, 543.

PERSONNEL MOVEMENTS

STAFF

Arrivals

Europe

SARAZIN, Marc (F), Physicist/Engineer, 14.5.1984

SCHNEERMANN, Michael (D), Mechanical Engineer, 1.7.1984

Departures

Chile

RUBLEWSKI, Wilhelm (D), Senior Electronics Technician, 31.8.1984

FELLOWS

Departures

Europe

VALENTIJN, Edwin (NL), 30.4.1984

Chile

JENSEN, Kaare (DK), 30.6.1984

ASSOCIATES

Arrivals

Europe

KRAUTTER, Joachim (D), 1.6.1984

Departures

Europe

IYE, Masanori (Japanese), 31.7.1984

CHINCARINI, Guido (Italian), 10.8.1984

COOPERANTS

Arrivals

Chile

SCHMIDER, Fran ois-Xavier (F), 9.4.1984

Departures

Chile

BOUVIER, Jer me (F), 31.5.1984

ALGUNOS RESUMENES

El Servicio de Coordinaci n Europea para el Telescopio Espacial comienza sus actividades

P. Benvenuti, ST-ECF

El d a 23 de febrero de 1983 los Directores Generales del Observatorio Europeo y de la Agencia Espacial Europea firmaron un Convenio para crear el Servicio de Coordinaci n Europea para el Telescopio Espacial (ST-ECF). Un a o m s tarde, el d a 1  de marzo de 1984, el ST-ECF inici  sus actividades en el edificio de la ESO en Garching.

ESO, the European Southern Observatory, was created in 1962 to . . . establish and operate an astronomical observatory in the southern hemisphere, equipped with powerful instruments, with the aim of furthering and organizing collaboration in astronomy . . . It is supported by eight countries: Belgium, Denmark, France, the Federal Republic of Germany, Italy, the Netherlands, Sweden and Switzerland. It operates the La Silla observatory in the Atacama desert, 600 km north of Santiago de Chile, at 2,400 m altitude, where thirteen telescopes with apertures up to 3.6 m are presently in operation. The astronomical observations on La Silla are carried out by visiting astronomers – mainly from the member countries – and, to some extent, by ESO staff astronomers, often in collaboration with the former. The ESO Headquarters in Europe are located in Garching, near Munich. ESO has about 120 international staff members in Europe and Chile and about 120 local staff members in Santiago and on La Silla. In addition, there are a number of fellows and scientific associates.

The ESO MESSENGER is published four times a year: in March, June, September and December. It is distributed free to ESO personnel and others interested in astronomy. The text of any article may be reprinted if credit is given to ESO. Copies of most illustrations are available to editors without charge.

Editor: Philippe Véron
 Technical editor: Kurt Kjär

EUROPEAN
 SOUTHERN OBSERVATORY
 Karl-Schwarzschild-Str. 2
 D-8046 Garching b. München
 Fed. Rep. of Germany
 Tel. (089) 32006-0
 Telex 5-28282-0 eo d

Printed by Universitätsdruckerei
 Dr. C. Wolf & Sohn
 Heidemannstraße 166
 8000 München 45
 Fed. Rep. of Germany

ISSN 0722-6691

El propósito primordial del ST-ECF es de aumentar dentro de Europa las capacidades del uso científico del Telescopio Espacial y de su archivo de datos. En efecto, el ST-ECF será el centro europeo para las actividades relacionadas con el ST: coordinará el desarrollo del análisis de datos software relacionados con el ST en Europa y el Instituto Científico del Telescopio Espacial en los Estados Unidos, desarrollará un nuevo software de aplicación para la reducción y el análisis de datos del ST, creará un método eficaz para archivar, catalogar, recuperar y propagar los datos no pertenecientes al ST, proporcionará una apropiada fuente de información detallada en Europa sobre los métodos de operación y ejecución

del Telescopio Espacial y de su instrumental científico complementario.

Actualmente, el limitado personal del ST-ECF está compuesto por el Jefe (el autor), anteriormente Contralor del Observatorio IUE en VILSPA, Madrid, el Jefe Adjunto, Dr. Rudolf Albrecht, anteriormente en el Instituto Científico del Telescopio Espacial, y la secretaria, Srta. Britt Sjöberg. El Dr. T. Courvoisier fué nombrado como uno de los científicos para la Información sobre Instrumentación y tomará su cargo a partir de junio. Todas las demás vacantes han sido publicadas y están caminando las actividades para emplear personal; esperamos completar el personal a mediados de 1985.

Cometa P/Crommelin 1983 n observado en ESO

A. C. Danks, ESO

El cometa P/Crommelin tiene un período de aproximadamente 27.4 años y consecuentemente tiene una órbita bastante bien estudiada. Se reconoció que Crommelin sería un buen objeto de ensayo para la red Internacional de Observadores de Halley (IHW).

Durante los meses de marzo y abril el cometa se encontraba especialmente bien ubicado para ser observado en el hemisferio sur. Por lo tanto, los astrónomos visitantes al telescopio de 3.6 m, Dr. J. Lub y R. de Grijp de Leiden, gentilmente accedieron incluir Crommelin en su lista de objetos de observación e hicieron espectros durante las noches del 8 y 9 de Marzo.

Al mismo tiempo también el Dr. D. Cesarsky del Instituto de Astrofísica de

Paris tomó un espectro en el telescopio de 2.2 m en La Silla. Igualmente muchos otros astrónomos visitantes tomaron espectros o efectuaron fotometría.

Así se obtuvieron algunos interesantes resultados que nos ayudan a comprender mejor la composición química del cometa. Pero, lo que es aun más importante, estas observaciones han demostrado que con la cooperación de astrónomos visitantes se pueden lograr interesantes y valiosas observaciones de cometas.

La figura 2 en la página 10 muestra una fotografía del cometa tomada por H.E. Schuster con el telescopio Schmidt. La línea en la fotografía fue producida por un satélite que cruzaba el campo durante la exposición.

Contents

P. Benvenuti: The Space Telescope European Coordinating Facility Begins its Activity	1
G. Lund and R. Ferlet: Progress in High Resolution Spectroscopy Using a Fibreoptic Coudé Link	2
Tentative Time-table of Council Sessions and Committee Meetings in 1984	3
A. Spaenhauer and F. Thévenin: Spectroscopy of Late Type Giant Stars	6
S. Ortolani and R. Gratton: Deep Photometry of Far Globular Clusters	7
A.C. Danks: Comet P/Crommelin 1983 n	9
G. Alcaíno and W. Liller: The Pickering-Racine Wedge with the Triplet Corrector at the ESO 3.6 m Telescope	10
M. Azzopardi and B.E. Westerland: Finding Carbon Stars in Nearby Galaxies	12
List of Preprints Published at ESO Scientific Group (March – May 1984)	15
J.V. Feitzinger and J.A. Stüwe: A Catalogue of Dark Nebulae for the Southern Hemisphere	16
F. Matteucci: The Chemical Enrichment of Galaxies	17
E. Fossat, G. Grec, B. Gelly and Y. Decanini: Stellar Seismology: Five-Minute P Modes Detected on Alpha Centauri	20
D.R. Soderblom: A Close Look at Our Closest Neighbor: High Resolution Spectroscopy of Alpha Centauri	22
A.E. Ringuelet and J. Sahade: Ca II in HD 190073 Revisited	23
J. Brand: Determination of the Rotation Curve of Our Galaxy. Observations of Distant Nebulae	26
R. Beck, R.-J. Dettmar, R. Wielebinski, N. Loiseau, C. Martin and G.F.O. Schnur: Optical Haloes Around Galaxies	29
Personnel Movements	31
Algunos Resúmenes	31